New remains of *Condorchelys antiqua* (Testudinata) from the Early-Middle Jurassic of Patagonia: anatomy, phylogeny, and paedomorphosis in the early evolution of turtles

Juliana Sterli, Marcelo S. de la Fuente & Guillermo W. Rougier

View supplementary material

Published online: 26 Mar 2019.

Submit your article to this journal

View Crossmark data

Check for updates

ARTICLE

NEW REMAINS OF *CONDORCHELYS ANTIQUA* (TESTUDINATA) FROM THE EARLY-MIDDLE JURASSIC OF PATAGONIA: ANATOMY, PHYLOGENY, AND PAEDOMORPHOSIS IN THE EARLY EVOLUTION OF TURTLES

JULIANA STERLI,[*1] MARCELO S. DE LA FUENTE,[2] and GUILLERMO W. ROUGIER[3]

[1]CONICET–Museo Paleontológico Egidio Feruglio, Av. Fontana 140, 9100 Trelew, Chubut, Argentina, jsterli@mef.org.ar;
[2]CONICET–Grupo Vinculado al IANIGLA CCT Mendoza, Museo de Historia Natural de San Rafael, Parque Mariano Moreno s/n, 5600 San Rafael, Mendoza, Argentina, mdelafuente1910@gmail.com;
[3]Department of Anatomical Sciences and Neurobiology, School of Medicine, University of Louisville, 511 South Floyd, Louisville, Kentucky 40202, U.S.A., grougier@louisville.edu

ABSTRACT—New cranial and postcranial remains of the Early–Middle Jurassic turtle, *Condorchelys antiqua*, are described here in detail, providing new insights into the early evolution of turtles. Unconstrained and constrained cladistic analyses in addition to newly developed total-evidence Bayesian analysis were performed to explore large-scale turtle relationships and evolutionary trends. All the analyses show a similar resolution at the base of the tree, recovering several species of small-sized, fresh water turtles of the Early–Middle Jurassic at the base of the tree following the most basal, large-sized, terrestrial turtles from the Late Triassic. The calibration of the cladistic analyses and the tip-dating analysis provided similar results in the main nodes Testudines, Pan-Cryptodira, Cryptodira, Pan-Pleurodira, and Pleurodira, corroborating that the Jurassic is a key period for turtle evolution. The significant reduction in size in Early–Middle Jurassic stem turtles and the combination of certain characters (e.g., presence of fontanelles, loss of bones, loss of scutes) shown by those taxa suggests heterochronic changes, paedomorphosis in particular, at the base of the turtle tree. These morphological novelties could have trigged, or facilitated, the occupation of the aquatic niche as seen in Jurassic stem turtles.

SUPPLEMENTAL DATA—Supplemental materials are available for this article for free at www.tandfonline.com/UJVP

INTRODUCTION

All known specimens of *Condorchelys antiqua* were found in outcrops of the Lower–Middle Jurassic Cañadón Asfalto Formation (Cúneo et al., 2013, but see also Volkheimer et al., 2015), central Patagonia, Chubut Province, Argentina. *Condorchelys antiqua* was named and briefly described by Sterli (2008) and its phylogenetic relationships discussed. Later, Sterli and de la Fuente (2010) published a detailed description of the cranial and postcranial remains available at the time. One of us (G.W.R.) recovered all previous materials of *C. antiqua* while quarrying at the type locality of Queso Rallado (Rauhut et al., 2002) as part of microfossil collecting. Recent work at the quarry led to the discovery of new specimens of *C. antiqua* representing previously unknown skeletal elements and a partial associated skeleton that allows assigning isolated specimens to *C. antiqua* and to substantiate previous referrals. The new specimens provide novel information about the anatomy of the skull roof, basicranium, and, mainly, about the postcranium (e.g., shell, girdles, limb bones). Preliminary results on the implications of these new findings of *C. antiqua* were previously reported by Sterli et al. (2015a). The histology and paleoecology of *C. antiqua* was presented by Cerda et al. (2016).

There are few taxa whose anatomy, presumed phylogenetic position, and age are comparable to *C. antiqua*. In this study, *C. antiqua* is primarily compared with *Kayentachelys aprix* Gaffney, Hutchison, Jenkins, and Meeker, 1987, *Indochelys spatulata* Datta, Manna, Ghosh, and Das, 2000, *Eileanchelys waldmani* Anquetin, Barrett, Jones, Moore-Fay, and Evans, 2009, *Heckerochelys romani* Sukhanov, 2006, and the recently discovered *Sichuanchelys palatodentata* Joyce, Rabi, Clark, and Xu, 2016. Although some of these species preserve cranial and postcranial remains, descriptions and illustrations have focused on the skull and shell. Other postcranial remains, such as girdles, limb bones, and vertebrae, have received much less attention in previous studies.

The emblematic Early Jurassic *Kayentachelys aprix* (Kayenta Formation, U.S.A.) has been in the eye of the storm of the two competing phylogenetic hypotheses about turtle evolution. Gaffney and colleagues (e.g., Gaffney et al., 1987; Gaffney and Jenkins, 2010; Gaffney, 1996) argued that *K. aprix* is the oldest cryptodiran turtle, whereas for Joyce and colleagues (e.g., Joyce, 2007; Sterli, 2008; Anquetin, 2011; Sterli et al., 2013) *K. aprix* is stem- to crown-group Testudines. *Kayentachelys aprix* is known from cranial and postcranial remains (Gaffney et al., 1987); however, only the skull has been described in detail (Gaffney et al., 2007; Sterli and Joyce, 2007).

Indochelys spatulata is known by a single specimen from the Kota Formation (Early Jurassic) in India (Datta et al., 2000). The fossil includes the carapace and the internal mold of the

plastron with some postcranial remains. On the contrary, several specimens with cranial and postcranial remains are known for *E. waldmani* (Anquetin et al., 2009; Anquetin, 2010, 2011) from the Middle Jurassic (Bathonian) of the Isle of Skye (Scotland). *Heckerochelys romani* was recovered in Middle Jurassic rocks from Russia (Sukhanov, 2006). Several specimens with cranial and postcranial remains have been attributed to this species; unfortunately, only part of the skull and the shell have been figured (Sukhanov, 2006).

The recently published turtle from the Late Jurassic of China, *Sichuanchelys palatodentata*, is represented by several nicely preserved specimens with cranial and postcranial remains (Joyce et al., 2016). Joyce et al. (2016) provided a detailed anatomical description and concluded that *S. palatodentata* is phylogenetically related to *Mongolochelys efremovi* Khosatzky, 1997 (from the Late Cretaceous of Mongolia). On the other hand, in previous cladistic analyses (e.g., Sterli, 2008, 2010), *C. antiqua*, *K. aprix*, and *I. spatulata* have been recovered in an unresolved polytomy at the base of a broad turtle phylogeny, but more derived than Triassic turtles. *Heckerochelys romani* and *E. waldmani* were both recovered in a more derived position (e.g., Sterli, 2008, 2010).

Here, we describe new specimens of *C. antiqua* and restudy reprepared specimens previously published. The new information is included in a series of cladistic analyses and in novel total-evidence Bayesian analysis to evaluate its impact on our understanding of early turtle evolution and on the phylogenetic position of *C. antiqua*. Additionally, we explore the evolution of size in a cladistic context, evaluating its significance using statistics. Furthermore, we discuss the possibility that heterochronic processes, especially paedomorphosis, could have driven the early evolution of turtles.

Institutional Abbreviation—**MPEF-PV**, Vertebrate Paleontology Collection, Museo Paleontológico Egidio Feruglio, Trelew, Chubut, Argentina.

Anatomical Abbreviations—**AB**, abdominal scute; **ac**, acetabulum; **bo**, basioccipital; **bpp**, basipterygoid process; **bs**, basisphenoid; **cap**, capitellum; **cc**, centrum cotyle; **ch**, chevron; **cm**, condylus mandibularis; **co**, costal; **coc**, condylus occipitalis; **cor**, coracoid; **ct**, cavum tympani; **dpc**, deltopectoral crest; **ect**, ectepicondyle; **ecf**, ectepicondyle foramen; **ent**, entepicondyle; **FE**, femoral scute; **fem**, femur; **fi**, fibula; **fpccc**, foramen posterius canalis carotici cerebralis; **fr**, frontal; **hh**, humeral head; **his**, hypoischium; **HU**, humeral scute; **hum**, humerus; **hyo**, hyoplastron; **hypo**, hypoplastron; **il**, ilium; **IM**, inframarginal scute; **is**, ischium; **itf**, intertubercular fossa; **iv**, interpterygoid vacuity; **lp**, lateral process; **MA**, marginal scute; **md**, musk ducts; **meso**, mesoplastron; **mp**, medial process; **mx**, maxilla; **ne**, neural; **na**, nasal; **nc**, neural crest; **nu**, nuchal; **op**, opisthotic; **up**, ungual phalanx; **pa**, parietal; **pe**, peripheral; **PEC**, pectoral scute; **pi**, processus interfenestralis of the opisthotic; **PL**, pleural scute; **po**, postorbital; **pt**, pterygoid; **prz**, prezygapophysis; **pu**, pubis; **pz**, postzygapophysis; **qu**, quadrate; **ra**, radius; **sc**, scapula; **sh**, shoulder; **sit**, secondary intertubercular fossa; **so**, supraoccipital; **ti**, tibia; **tp**, transverse process; **tr**, thoracic rib; **tro**, trochlea; **tv**, thoracic vertebra; **VE**, vertebral scute; **xi**, xiphiplastron.

MATERIALS AND METHODS

Materials

All the specimens of *C. antiqua* come from the Queso Rallado locality (Sterli and de la Fuente, 2010). Queso Rallado (Rauhut et al., 2002; Rougier et al., 2007) is located near Cerro Cóndor Village in Chubut Province (Argentina) in outcrops of the Cañadón Asfalto Formation (Stipanicic et al., 1968). Recent high-precision dating (Cúneo et al., 2013) showed that

the base of the Cañadón Asfalto Formation was deposited ca. 178.8 ± 1 million years ago (Mya; Toarcian, Early Jurassic), and the overlying Cañadón Calcáreo Formation was dated ca. 157.4 ± 0.05 Mya (Oxfordian, Late Jurassic), suggesting a Toarcian–Aalenian (maybe Bajocian) age for the Cañadón Asfalto Formation. Queso Rallado locality is located very low in the stratigraphic section (Rougier et al., 2007), and given the dominance of pyroclastic sediments, it clearly was under the same set of regional constrains that determined the character of the underlying volcanic Lonco Trapial Formation. Consequently, it is likely that the age of the fossils is in fact close to the lower limit of the dates provided for the Cañadón Asfalto Formation.

Phylogenetic Analysis

Cladistic Analyses—We used the matrix of López-Conde et al. (2017), which was the most up-to-date matrix available at the time we performed the analysis. The original matrix has 99 taxa and 245 characters (Supplementary Materials 1 and 2). The new specimens of *C. antiqua* (see above) allowed 23 previously unknown characters to be scored, reaching 51.6% completeness. The data set was analyzed in TNT (Goloboff et al., 2008). The search started with 1000 replicates producing Wagner trees, and they were perturbed with the algorithm Tree Bisection Reconnection (TBR). Later, all the most parsimonious trees (MPTs) found in the first round of TBR were perturbed again to look for all the MPTs. If more than one tree was found, a strict consensus tree was calculated. Bremer support, bootstrap, and jackknife were the branch supports estimated in TNT software. One thousand replicates were performed to calculate bootstrap and jackknife. The synapomorphies common to all the MPTs were identified. We have performed two kinds of analyses, one unconstrained (more conservative approach) and the other constrained using molecular scaffolds as suggested by Crawford et al. (2015). Furthermore, we performed two constrained analyses using the most up-to-date molecular topologies: Crawford et al.'s (2015) and Guillon et al.'s (2012) topologies (see Supplementary Material 3).

If several polytomies are found in the strict consensus tree, this could be caused by the presence of wild-card taxon/taxa. To explore the presence of unstable taxon/taxa, the script iterPCR (Pol and Escapa, 2009) was run in TNT. This script finds the unstable taxa and the reasons why those taxa are unstable (conflict of characters or missing data). The trees were calibrated using the script MSM (Pol and Norell, 2006) and then modified with Illustrator to reproduce the topology of the strict consensus. The age of each taxon can be found in Supplementary Material 4. The matrix used to calibrate the phylogeny is in Supplementary Material 5.

Bayesian Analysis—Model-based analyses that combine morphological and molecular data in a total-evidence approach represent a powerful new method that allows tree topology, divergence dates, and evolutionary rates to be estimated simultaneously (Beck et al., 2016; Pyron, 2016). We performed a total-evidence analysis by combining the morphological matrix used for maximum parsimony (MP) with the genomic database used by Sterli (2010), which includes the mitochondrial and nuclear genes 12S, 16S, Cytb, Rag1, and R35. Partitions for the molecular data and appropriate models were recognized using PartitionFinder 1.1.1 (Lanfear at al., 2012); nuclear genes were initially partitioned by genes and codons under the assumption of linked branch lengths. Because the goal was to run the analysis in MrBayes, only models implemented by MrBayes 3.2.X were considered and heuristically tested using the 'Greedy' search algorithm; the Bayesian information criterion (BIC) was

the optimality criterion for model selection. Partitions and models selected can be seen in the Supplementary Material 6. The morphological partition we used is the one recently developed and arguably the more realistic model of discrete morphological character evolution (MkA), in which unequal (asymmetric) transition rates for binary characters can be used where polarity can be identified a priori (Pyron, 2016). This model is a refinement of the classical Mk model developed by Lewis (2001), and it was implemented in MrBayes 3.2.6. The morphological matrix was divided into two partitions. The MkA model was applied to the partition formed by all the binary characters for which the ancestral/derived state could be determined/assumed. The MK model was applied to the partition formed by the multistate characters and to binary characters of ambiguous polarity. We implemented a Bayesian total-evidence approach (Ronquist et al., 2012; Beck and Lee, 2014; Beck et al., 2016; Pyron, 2016) and used a combination of tip and node dating under birth-death models of branching, extinction, and sampling (Heath et al., 2014; Dos Reis, 2016; Zhang et al., 2015).

For the tip-dating and tip-and-node-dating analyses, we used the 'fossilized birth-death' topology prior (accounting for incomplete sampling of extant taxa), which outperforms uniform priors and diversified sampling (Zhang et al., 2016). Each recent taxon was given a fixed date of 0 million years, and the extinct taxa were dated using a uniform prior for the best age estimates available. Groups for which reasonably resolved hypotheses of relationships are available were constrained, and the age of the group determined by the oldest member of the group as recovered by previous studies. The composition of the constrained groups and age distributions are provided in Supplementary Materials 3 and 6. The priors were introduced as offset exponential distributions, with a minimum determined by the age of fossil/youngest member and a corresponding mean that was heuristically found to produce a 95% age distribution that coincided with the maximum expected age (Supplementary Material 6). The total tree height (tree root) was established as a uniform probability function between 320 and 333 to the base of the Pennsylvanian, effectively determining a conservative maximum possible age for turtles substantially older than any currently accepted age.

The MrBayes analysis was run with 4 chains for 50 million generations using the default heat parameters in the CIPRES cluster (Miller et al., 2010); most runs were completed in about 3 days. The burn-in fraction was set at 50% after ensuring that convergence had been achieved. The results were summarized as a maximum clade credibility tree (TreeAnnotator, BEAST package), with 95% highest posterior density intervals on the divergence times.

Size Evolution

We also explored the evolution of size in turtles as documented by the taxa included in our matrix. Size for each taxon is provided in Supplementary Material 4. We first mapped the size as a continuous character in TNT (Supplementary Material 5), then we documented for each taxon and node their ancestral size as optimized by TNT (Supplementary Material 3). If a size range was obtained in a node, the average was used as ancestral size. To test whether the ancestral and final sizes are significantly different, we applied the new technique developed by Vlachos and Rabi (2017). Following their approach, the sample of sizes and ancestral sizes were analyzed statistically to test normal distribution and correlation between them, and with a regression analysis using LOESS (locally weighted scatterplot smoothing) model (PAST 3 by Hammer

et al., 2001). Taxa or nodes that were recovered outside the 95% confidence interval of the regression analysis were interpreted as having potentially significant differences between their final and ancestral sizes (Vlachos and Rabi, 2017).

Character Evolution

We also mapped several characters that have been included in the cladistic analysis (e.g., presence of lacrimal, presence of supratemporal) to see their evolution. Furthermore, we mapped the 'habitat' of each taxon (Supplementary Material 7) to explore plausible ecological/habitat use correlation with the evolution of size.

SYSTEMATIC PALEONTOLOGY

TESTUDINATA Klein, 1760 (sensu Joyce et al., 2004)
MESOCHELYDIA Joyce, 2017
CONDORCHELYS ANTIQUA Sterli, 2008

Holotype—MPEF-PV 1152, basicranium.
Type Locality and Horizon—Queso Rallado locality (43°24′S, 69°13′W), Cerro Cóndor Village, Chubut Province, Argentina (Rauhut et al., 2002; Rougier et al., 2007). Toarcian–Aalenian (?Bajocian), Early–Middle Jurassic (Cúneo et al., 2013).
Referred Material—Referred specimens listed in Sterli and de la Fuente (2010) plus MPEF-PV 1784, right humerus; MPEF-PV 3133c, coracoid; MPEF-PV 3148, coracoid; MPEF-PV 3149, left humerus and a caudal vertebra; MPEF-PV 3150, distal end of right humerus; MPEF-PV 3151, proximal end of right humerus; MPEF-PV 3152, proximal end of right femur; MPEF-PV 3153, proximal end of right humerus; MPEF-PV 3158, caudal vertebra; MPEF-PV 10884, partial shell and associated postcranium; MPEF-PV 10900, skull.

DESCRIPTION

The following description is based on the information provided by the new specimens listed above. For further information on previously described specimens, see Sterli (2008) and Sterli and de la Fuente (2010).

Skull

The description of the skull presented here is based on specimen MPEF-PV 10900, and is intended to complement information presented previously from MPEF-PV 1152, 1998, and 3131. The new specimen is a compressed skull, with some bones from the periphery of the skull missing. The preserved bones are described below.

Dermal Roof Elements—Based on comparisons with other basal turtles (e.g., *Progranochelys quenstedti*, *K. aprix*, *E. waldmani*), the nasal of *C. antiqua* (Fig. 1) is likely the most anterior bone from the skull roof preserved in this specimen. Only the posteromedial part of the nasals is preserved; it contacts the frontal and its counterpart medially. Other relationships have been lost. The nasals are wedged posteriorly between the frontals, having a ventral process that forms the lateral wall of the sulcus olfactorius. The nasal portion of the sulcus olfactorius is broad as in *Kayentachelys aprix* (Sterli and Joyce, 2007), but its posterior continuation in the frontal does not narrow posteriorly as it does in *K. aprix* (Sterli and Joyce, 2007).

Both frontals are preserved and almost complete (Fig. 1). The frontal is a large bone in the skull roof of *C. antiqua*, contacting the nasal anteriorly, the parietal posteriorly, the
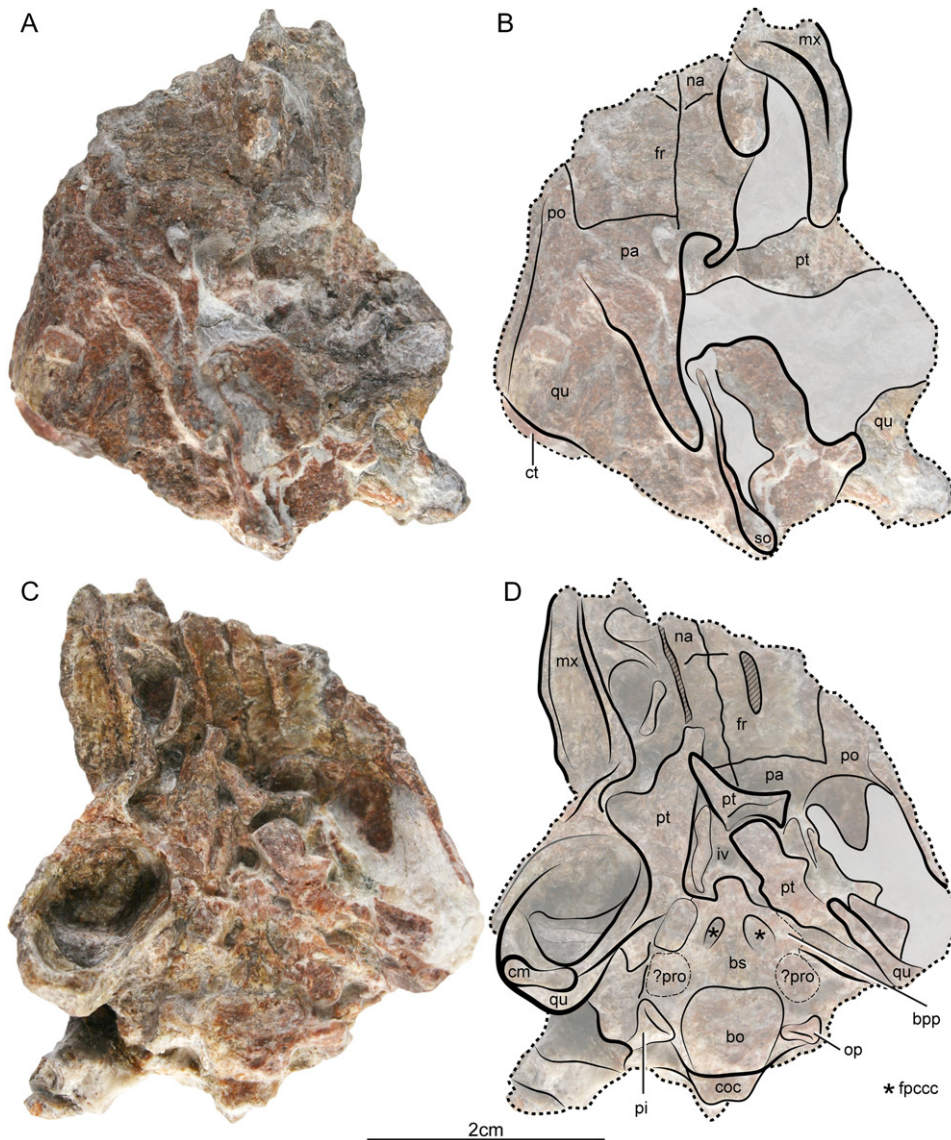
FIGURE 1. *Condorchelys antiqua* MPEF-PV 10900, Queso Rallado, Chubut Province, Argentina; Cañadón Asfalto Formation, Toarcian–Bajocian (?Bathonian). **A**, photograph of the dorsal view of the skull; **B**, drawing of the dorsal view of the skull; **C**, photograph of the ventral view of the skull; **D**, drawing of the ventral view of the skull. Dashed lines indicate broken edges. Dotted and dashed lines indicate possible limits of the bone.

postorbital posterolateraly, and its counterpart medially. The frontal has a ventral process that forms the lateral wall of the sulcus olfactorius (see above). Well-developed parasagittal ridges delimiting the sulcus olfactorius such as those described by Sterli and Joyce (2007) in *K. aprix* are present in *C. antiqua*. These ridges are subparallel in *C. antiqua* and do not form an hourglass-shaped sulcus olfactorius as in *K. aprix*. Unfortunately, the nature of our specimen prevents observing whether the frontal formed part of the orbital rim or the presence of a potential contact with the prefrontal.

Only small pieces of both parietals (Fig. 1) can be recognized in this specimen, preventing any detailed description. Only the anterior contact with the frontal is preserved; contacts of the frontal with the postorbital laterally and with the supraoccipital posteromedially are assumed.

Only a small portion of the left postorbital (Fig. 1) is preserved, maintaining its medial contact with the frontal and evading further description.

Palatal Elements—The right maxilla (Fig. 1) as preserved is almost complete but displaced from its natural position. It is evident that the maxilla formed at least the anteroventral rim of the orbit and the triturating surface. The anterodorsal process of the maxilla is well preserved. Ventrally, the well-preserved triturating surface is wide, slightly concave, and delimited by a lingual (medially) and a labial (laterally) ridge of equal height and length. A different condition is seen in *K. aprix* where the lingual ridge is shorter and lower than the labial one. Contrary to *K. aprix*, in *C. antiqua* the lingual and labial ridges are subparallel. There is no evidence of a medial ridge in *C. antiqua*. The triturating surface is not available in any specimen of *Eileanchelys waldmani*.

Palatoquadrate Elements—Both quadrates are preserved (Fig. 1). The lateral and dorsal surfaces of the left quadrate are in better conditions, whereas the ventral morphology is more complete in the right quadrate. The only clear suture of the quadrate is the one with the pterygoid medially. Based on its

general morphology and comparison with other basal turtles, we believe that it is likely that the quadrate also contacted the prootic medially and the opisthotic posteriorly. Unfortunately, the sutures with the parietal and/or supraoccipital cannot be determined. The quadrate forms a deep and well-developed cavum tympani in *C. antiqua*. The right quadrate bears the condylus mandibularis ventrally. The articular area is rectangular, wider than long, subdivided in two surfaces, one medial and one lateral, both of which are slightly convex. Contrary to the condition seen in *K. aprix*, the medial surface is almost subequal or slightly longer than the lateral one. In *Eileanchelys waldmani*, both articular surfaces are separated by an anteroposterior groove and the medial articular facet is slightly concave (Anquetin, 2010).

Both pterygoids are preserved (Fig. 1), with the right pterygoid being in better condition, but preserving only its posterolateral contact with the quadrate. The pterygoid has a triradiate shape with anterior, lateral, and posterolateral processes. The anterior process forms the lateral border of the well-developed, triangular interpterygoid vacuity. The lateral process is well developed and contacted the lateral wall of the skull (e.g., jugal or quadratojugal). There is neither a posterior process of the lateral process of the pterygoid nor a vertical flange. The posterolateral process (quadrate process of the pterygoid) is a vertical lamina that abuts the pterygoid process of the quadrate on its anterolateral surface. The quadrate process of the pterygoid does not develop a posterior flat process as seen in pan-cryptodirans, resulting in ventral exposure of the prootic. There are no pterygoid teeth in *C. antiqua*, contrary to the condition seen in *K. aprix* and more basal turtles (i.e., *Pr. quenstedti*).

Braincase Elements—Only a small strip of the supraoccipital is preserved in the skull (Fig. 1), representing a remnant of the supraoccipital crest. Unfortunately, no further description is possible.

The basioccipital (Fig. 1C, D) is a block-like element, with poorly preserved contacts, the anterior one with the basisphenoid is recognizable, but those with the opisthotic and exoccipital are assumed. The basioccipital forms the condylus occipitalis, which is slightly oval, being wider than high.

Remains of both prootics are preserved (Fig. 1C, D); however, the deficient preservation does not allow a detailed description, besides the fact that they are small, solid elements with, at present, no identifiable contacts.

Remnants, mostly of the proximal portions, of both opisthotics are preserved (Fig. 1C–D). In the right opisthotic, a robust processus interfenestralis is seen, similar in proportions to that of *K. aprix* (Sterli and Joyce, 2007). Conversely, the development of the process of the opisthotic in *E. waldmani* (Anquetin, 2010) and *Hecherochelys romani* (Sukhanov, 2006) is intermediate between the robust structure recognized in basal turtles and the slender bone characteristic of crown-group turtles.

Basisphenoid—Most of the basisphenoid is preserved, but the only clear contact is the posterior one with the basioccipital. The contacts with the pterygoid and prootic are reconstructed. Only the ventral view of the basisphenoid is available in the new specimens. The foramen posterius canalis carotici cerebralis is preserved in the ventral view of the basisphenoid and located anteriorly between the basitrabecular processes in a big, oval depression. A similar position of these foramina is observed in other basal turtles such as *Pr. quenstedti*, *K. aprix*, and *H. romani* (Gaffney, 1990; Sukhanov, 2006; Sterli and Joyce, 2007). Only the base of the rostrum basisphenoidale is preserved anteriorly and in connection with the pterygoid. There is a slit between the rostrum and the pterygoid through which the palatine artery would have entered the skull. On

both sides of the foramen posterius canalis carotici cerebralis, a ventral protrusion of the basisphenoid is observed, regarded here as the basipterygoid processes.

Shell and Postcranium

The description in this section is based mainly on specimen MPEF-PV 10884. Parts of the descriptions were enhanced with information provided by other specimens (MPEF-PV 1783a–c, 1784, 3132–3136, 3147–3153, 3158–3160, and 10901). Those additional specimens are mentioned in the text when appropriate. The bony plates of the shell (both carapace and plastron) are slightly ornamented with very small grooves and pits that are difficult to observe with the naked eye. Measurements of the carapace, plastron, and limb bones are provided in Appendix 1.

Carapace—The new specimen described here, MPEF-PV 10884 (Figs. 2–3), together with previously known specimens (e.g., MPEF-PV 1783a–c, 3132, 3134) allowed us to provide a reconstruction of the shell (Fig. 5). The estimated straight carapace length of MPEF-PV 10884 is 21 cm. It is oval, being longer (21 cm approximately) than wide (16 cm approximately). This outline is likely similar to the shape figured by Gaffney et al. (1987) for *K. aprix*. Conversely, a different shape with sharp, tapering posterolateral margins is present in *E. waldmani* and in *Indochelys spatulata* (Datta et al., 2000; Anquetin, 2010). As in other specimens of *C. antiqua* (see Sterli and de la Fuente, 2010), the carapace bones of the specimen described herein are ornamented with small pits and small grooves.

Regarding the bony plates, most of the nuchal is preserved, missing only the most anterior part and portions of the left edge (Fig. 2A, B). Due to the incompleteness of the specimen, we cannot assess whether there was a nuchal notch as in *Kayentachelys aprix* (Gaffney et al., 1987) or whether it was absent as in *Eileanchelys waldmani* (Anquetin, 2010). Although the sutures with the peripherals cannot be recognized, it appears that the nuchal is wider than long. It contacts costal 1 posterolaterally and neural 1 posteromedially.

Neurals 1 to 8 are preserved in this specimen (Fig. 2A, B). They are generally rectangular in shape, and longer than wide as in *E. waldmani* and *I. spatulata*. Neural 1 is the largest preserved, followed by the third, whereas neural 7 is the smallest. Neural 1 contacts the nuchal anteriorly and costals 1 and 2 laterally. Neural 2 contacts costal 2 laterally. Neural 3 contacts costals 3 and 4 laterally, neural 4 contacts costal 4 laterally, neural 5 contacts costals 4 and 5 laterally, neural 6 contacts costal 6 laterally, and neural 7 contacts costals 6 and 7 laterally. Only the anterior-most portion of neural 8 is preserved, preventing any further description. Costals 1 to 7 from both sides are preserved (Fig. 2). They are wide elements and anteroposteriorly short. Costals 2, 4, and 5 expand distally, whereas costals 1, 3, and 6 narrow distally. Costal 1 contacts the nuchal anteromedially, neural 1 medially, and, at least, peripherals 2 and 3. The contact with peripheral 1 is not observed. Costal 2 contacts neurals 1 and 2 medially and peripherals 3 to 5 laterally. Costal 3 contacts neural 3 medially and peripherals 5 and 6 laterally. Costal 4 contacts neurals 3 to 5 medially and peripherals 6 and 7 laterally. Costal 5 contacts neural 5 medially and peripherals 7 and 8 laterally. Costal 6 contacts neurals 6 and 7 medially and peripherals 8 and 9 laterally. The only preserved contacts of costal 7 are with neural 7 medially and peripheral 9 laterally.

Right peripherals 1 to 7 and left peripherals 5 to 9 are preserved (Fig. 2). Unfortunately, the limits of peripheral 1 are not preserved. The lateral edges of peripherals 4 to 7 are curved upwards (guttered). The contacts of peripherals are described above in the discussion of the costals. The preserved
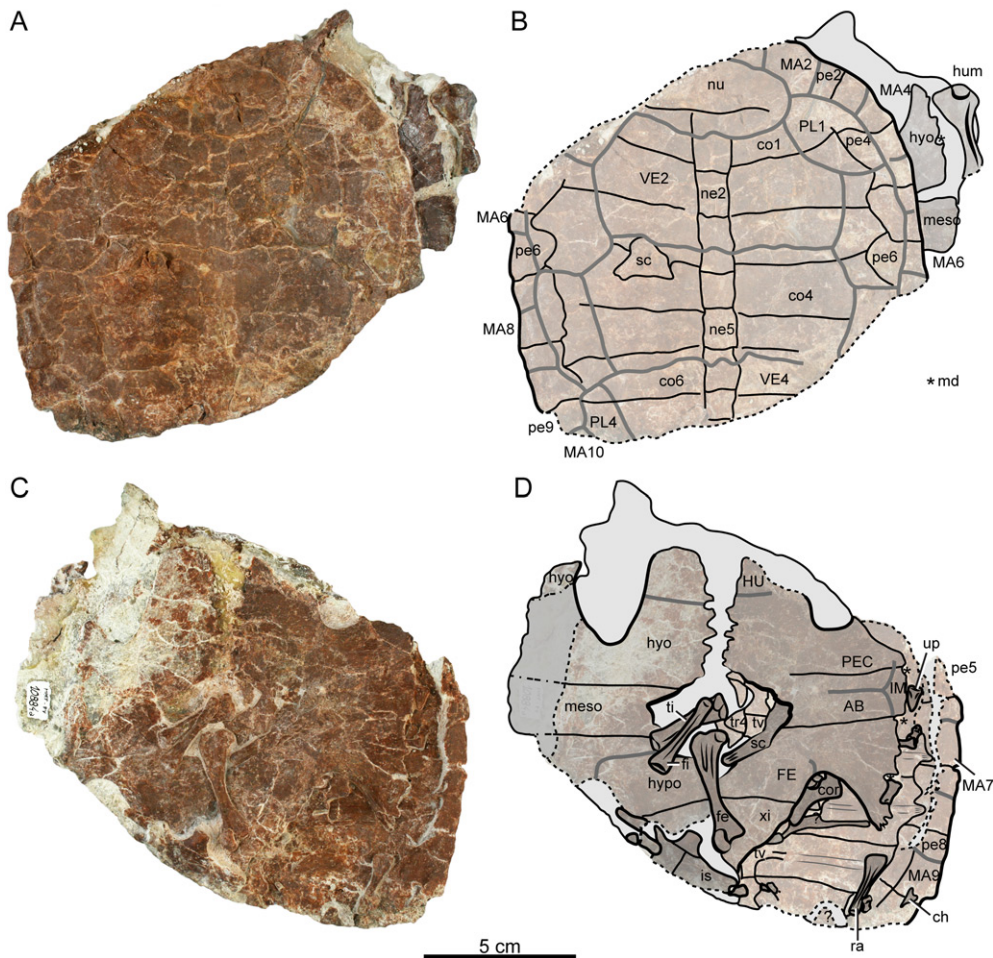
FIGURE 2. *Condorchelys antiqua* MPEF-PV 10884, Queso Rallado, Chubut Province, Argentina; Cañadón Asfalto Formation, Toarcian–Bajocian (?Bathonian). **A**, photograph of the dorsal view of the shell and associated postcranium; **B**, drawing of the dorsal view of the shell and associated postcranium; **C**, photograph of the ventral view of the shell and associated postcranium; **D**, drawing of the ventral view of the shell and associated postcranium. Dashed lines indicate broken edges.

peripherals are wide elements (mediolaterally), and they show a sinuous contact with the costals.

Regarding the scutes, vertebral scutes 1 to 4 are preserved (Fig. 2A, B). Vertebral 1 is the smallest and vertebral 3 is the largest preserved. Vertebrals 2 to 4 are twice wider than long, being notably larger than pleurals. The sulci between the vertebrals are sinuous (anterior inflection) when they cross the neurals. Vertebral 1 is oval, being wider than long. It covered at least part of the nuchal, and the anterior part of neural 1 and costal 1. Because the sutures in this anterolateral region of the carapace are not seen, the overlapping of vertebral 1 with peripherals cannot be determined. The contacts of vertebral 1 are, at least, with marginals 1 and 2 anterolaterally, with pleural 1 posterolaterally, and with vertebral 2 posteriorly. The sulcus between vertebrals 1 and 2 crosses neural 1. Vertebral 2 covered the posterior part of neural 1 and costal 1, costal 2, and the anterior part of neural 3 and costal 3. The sulcus between vertebrals 2 and 3 is located on neural 3. The contacts of vertebral 2 are with pleurals 1 and 2 laterally and with vertebrals 1 and 3 anteriorly and posteriorly, respectively. Vertebral 3 covered the posterior part of neural 3 and costal 3, neurals 4 and 5, costals 4 and 5, and the anterior part of neural 6 and costal 6. The sulcus between vertebral 3 and 4 is located on

neural 6 and costal 6. The contacts of vertebral 3 are with pleurals 2 and 3 laterally and with vertebrals 2 and 4 anteriorly and posteriorly, respectively. Vertebral 4 covered at least the posterior part of neural 6 and costal 6, neurals 7 and 8, and costal 7. The preserved contacts of vertebral 4 are with pleurals 3 and 4 laterally and with vertebral 3 anteriorly.

Right pleurals 1 to 3 and left pleurals 1 to 4 are preserved (Fig. 2A, B). In general, they are elongated elements, longer than wide. All the preserved pleurals covered the distal part of the costal bones and half width of the peripherals. Pleural 1 partially covered at least part of costals 1 and 2 and peripherals 2 to 4. It contacts vertebrals 1 and 2 medially, marginals 2 to 4 (maybe 5 as well) laterally, and pleural 2 posteriorly. Pleural 2 partially covered costals 2 to 4 and peripherals 4 to 6. It contacts vertebrals 2 and 3 medially, marginals 5 to 7 laterally, and pleural 1 and 3 anteriorly and posteriorly, respectively. Pleural 3 partially covered costals 4 to 6 and peripherals 7 and 8. It contacts vertebrals 3 and 4 medially, marginals 7 to 9 laterally, and pleural 2 and 4 anteriorly and posteriorly, respectively. Pleural 4 covered at least part of costals 6 and 7 and peripheral 9. Its preserved contacts are with pleural 3 anteriorly, with vertebral 4 medially, and with marginals 9 and 10 laterally.
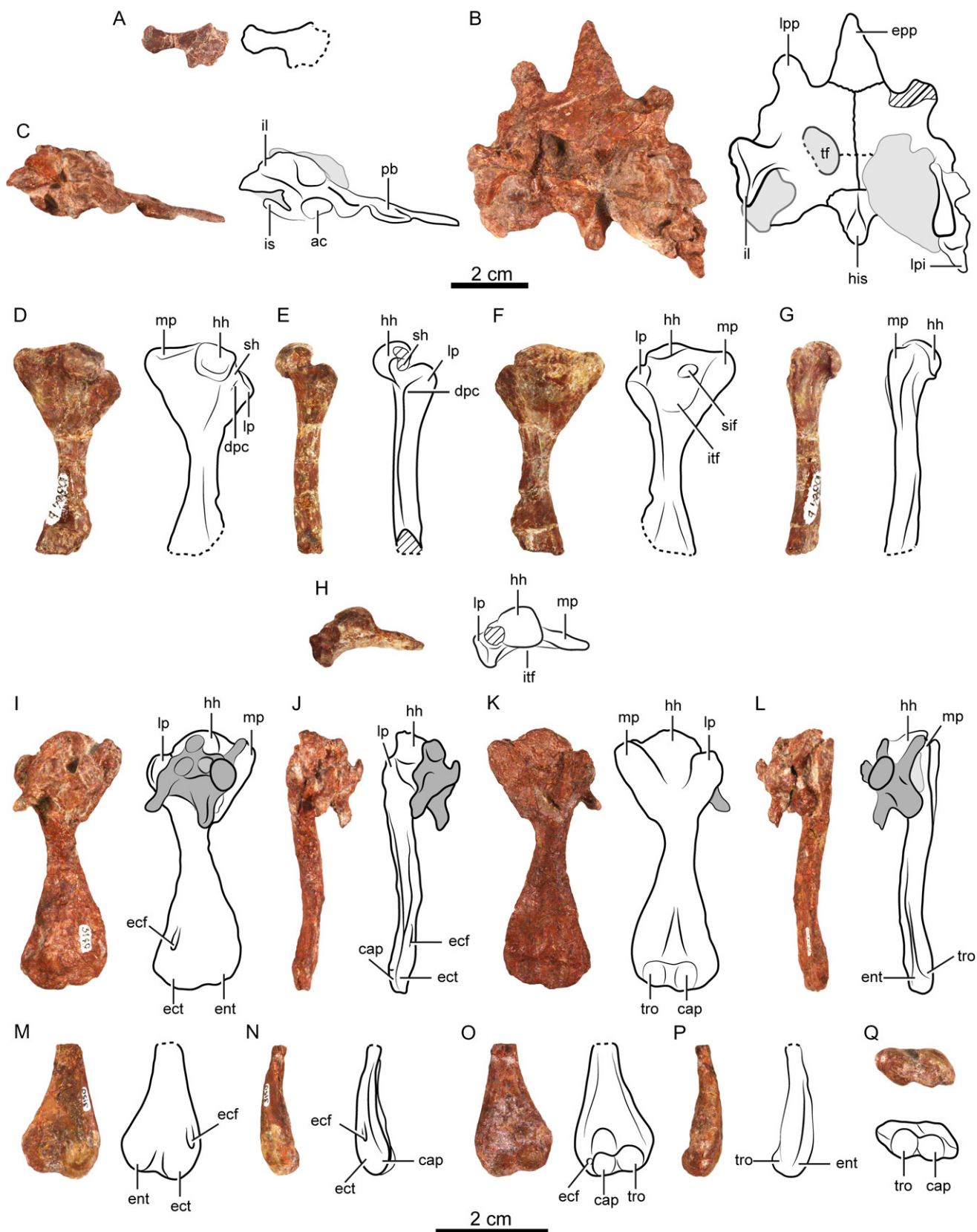
FIGURE 3. *Condorchelys antiqua*, Queso Rallado, Chubut Province, Argentina; Cañadón Asfalto Formation, Toarcian–Bajocian (?Bathonian). **A**, MPEF-PV 3133c, proximal end of coracoid; **B–C**, MPEF-PV 10901, pelvic girdle; **B**, dorsal view; **C**, right lateral view; **D–H**, MPEF-PV 10884, proximal end and diaphysis of a right humerus, in **D**, dorsal; **E**, anterior; **F**, ventral; **G**, posterior; and **H**, proximal views; **I–L**, MPEF-PV 3149, left humerus and caudal vertebra, in **I**, dorsal; **J**, anterior; **K**, ventral; and **L**, posterior views; **M–Q**, MPEF-PV 3150, distal end of a right humerus, in **M**, dorsal; **N**, anterior; **O**, ventral; **P**, posterior; and **Q**, distal views. Dashed lines indicate broken edges.
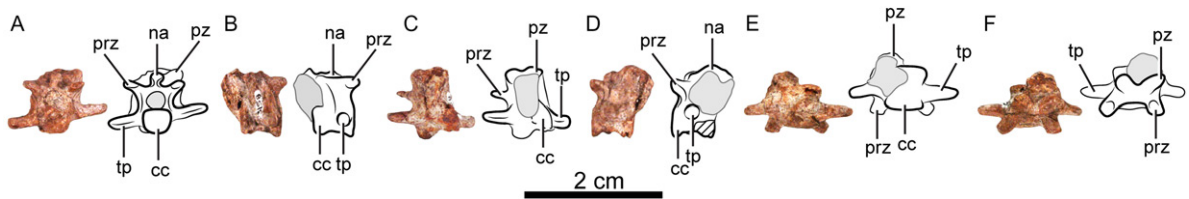
FIGURE 4. *Condorchelys antiqua*, Queso Rallado, Chubut Province, Argentina; Cañadón Asfalto Formation, Toarcian–Bajocian (?Bathonian). MPEF-PV 3158, caudal vertebra, in **A**, anterior; **B**, right lateral; **C**, posterior; **D**, left lateral; **E**, ventral; and **F**, dorsal views.

Right marginals 1 to 7 and left marginals 6 to 10 are preserved (Fig. 2). From marginal 4 (maybe 3) to marginal 10, the marginal scutes are restricted to the peripheral plates. There is only a small piece of marginal 1 preserved in the anterior part of the carapace, but no further description is possible. Marginals 2 and 9 are among the largest preserved marginals. Because the sutures of the anterior region of the carapace are not preserved, we cannot assess with certitude which bones are covered by marginal 2. Marginal 2 contacts marginal 1 anteromedially, vertebral 1 posteromedially, and pleural 1 posteriorly. Marginal 3 covered peripherals 2 and 3 and contacts pleural 1 medially. Marginal 4 covered peripherals 3 and 4 and contacts pleural 1 medially. Marginal 5 covered peripherals 4 and 5 and contacts pleural 2 medially. Marginal 6 covered peripherals 5 and 6 and contacts pleural 2 medially. Marginal 7 covered peripherals 6 and 7 and contacts pleurals 2 and 3 medially. Marginal 8 covered peripherals 7 and 8 and contacts pleural 3 medially. Marginal 9 covered peripherals 8 and 9 and contacts pleurals 3 and 4 medially. There is only a small portion of marginal 10; it covered at least part of peripheral 9, contacting anteriorly with marginal 9 and medially with pleural 4.

Plastron—Regarding the bony plates of the plastron, there are no remains of epiplastra or entoplastra preserved in the specimen MPEF-PV 10884 (Fig. 2C, D). However, one isolated entoplastron of *Condorchelys antiqua* (MPEF-PV 3134) was described by Sterli and de la Fuente (2010:fig. 6A, B).

Both hyoplastra are preserved (Fig. 2C, D), the right one being almost complete, missing only its most anterior part. In the left hyoplastron, the anterior part and portions of the axillary buttress are missing. The hyoplastron is the largest element of the plastron. It contacted the now missing epiplastra anteriorly, the entoplastron anteromedially, the mesoplastron posteriorly, the peripherals laterally, and their counterpart medially. The sutures between both hyoplastra and of the hyoplastron with the entoplastron are strongly interdigitated. An interdigitated suture is also present between the plastron and the carapace, suggesting a ligamentous attachment between them. On the other hand, the hyoplastron is tightly sutured with the mesoplastron. A central fontanelle, roughly rhomboidal, surrounded by hyoplastron, mesoplastron, and hypoplastron, is present.

Both mesoplastra are present in MPEF-PV10884 (Fig. 2C, D). They are rectangular, much wider than long. Each mesoplastron contacts the hyoplastron anteriorly, peripherals 5 and 6 laterally, and the hypoplastron posteriorly. In the medial part, the mesoplastron forms the border of the central plastral fontanelle.

Both hypoplastra are preserved (Fig. 2C, D). They are the second largest element of the plastron, contacting the mesoplastron anteriorly, peripherals 6 to 8 laterally, the xiphiplastron posteriorly, and its counterpart posteromedially. The hypoplastron forms the posterolateral border of the central plastral fontanelle.

Both xiphiplastra are preserved (Fig. 2C, D). The xiphiplastron contacts the hypoplastron anteriorly and its counterpart medially. The posterior part of the xiphiplastron is covered by the ischia and femur, not allowing detailed description.

Regarding the scutes of the plastron, only the part of the humeral scute that is covering the hypoplastron is present on both sides of the specimen (Fig. 2C, D). The humeropectoral sulci converge posteriorly towards the midline. The only preserved contact is the posterior one with the abdominal scute.

Both pectoral scutes are preserved; however, only the pectoroabdominal sulcus is seen in the left mesoplastron (Fig. 2C, D). The pectoral scute covered the hyoplastron and the mesoplastron, contacting the humeral scute anteriorly, the inframarginal laterally, the abdominal posteriorly, and its counterpart medially.

Both abdominal scutes are preserved (Fig. 2C, D). This scute covered the mesoplastron and the hypoplastron while contacting the pectoral scute anteriorly, the inframarginal scute laterally, the femoral scute posteriorly, and its counterpart medially.

Both femoral scutes can be recognized covering the hypoplastra and, perhaps, part of the xiphiplastra (Fig. 2C–D). The femoral contacts the abdominal scute anteriorly and its counterpart medially; the likely contact with the anal scute is not preserved.

Only one inframarginal scute is recognized on the left mesoplastron (Fig. 2C–D). It might correspond to inframarginal 3. It contacts the pectoral and abdominal scutes medially and marginal scutes 6 and 7 laterally.

Thoracic Vertebrae—Four thoracic vertebrae can be identified in specimen MPEF-PV 10884 (Fig. 2C, D). Two of them are seen through the central plastral fontanelle (probably thoracic vertebrae 4 and 5), and the other two (probably thoracic vertebrae 8 and 9) are located in the posterior part of the shell. All of them have hourglass-shaped vertebral bodies with flat articulating surfaces for the preceding and succeeding posterior thoracic vertebrae.

There are at least four thoracic ribs preserved in close relationship with the thoracic vertebrae (Fig. 2C–D). These thoracic ribs are here identified as the third and fourth from the right side and the seventh and eighth from the left side. The proximal end of the thoracic ribs is triangular, with the base contacting the thoracic vertebra. Thoracic rib 3 contacted, at least, thoracic vertebra 4, and the rib is attached to costal 2. Thoracic rib 4 has a small contact with the posterolateral part of thoracic vertebra 4 and a large contact with the anterolateral part of thoracic vertebra 5. It is clear that thoracic rib 8 contacts only thoracic vertebra 8.

Pectoral Girdle—A scapula and a coracoid are preserved in specimen MPEF-PV 10884 (Fig. 2D), corroborating the triradiate nature of the pectoral girdle for *Condorchelys antiqua* (Sterli and de la Fuente, 2010). One scapula is preserved; however, due to preservation (partially obscured by sediment), we cannot assess whether it is the right or the left scapula (Fig. 2C, D). A rod-like dorsal process is observed in the specimen.
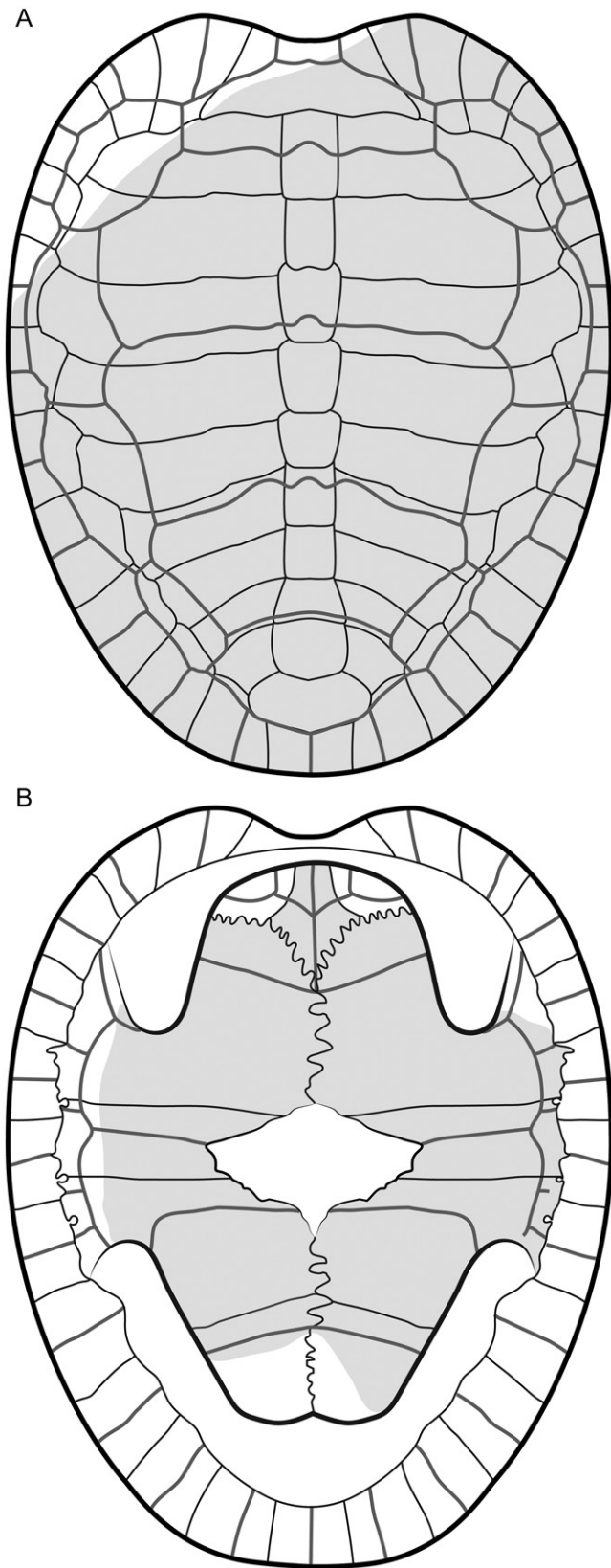
FIGURE 5. Reconstruction of the carapace and plastron of *Condorchelys antiqua* based on all available specimens (MPEF-PV 1783a–b, 3132, 3134, 3136, 3147, 3160, and 10884). **A**, dorsal view; **B**, ventral view. The known parts of the shell are highlighted in gray, and the unknown parts were reconstructed based on the reconstruction of *Kayentachelys aprix* made by Gaffney et al. (1987).

The distal end of the process is striated. The proximal end of the scapula is not seen in specimen MPEF-PV 10884.

One coracoid is preserved in MPEF-PV 10884; unfortunately, again due to preservation, we cannot assess whether it is the right or the left coracoid (Fig. 2C, D). The proximal end of the coracoid is preserved and forms part of the glenoid, whereas the distal end is expanded. Specimen MPEF-PV 3133c (Fig. 3A) is also identified as a coracoid, probably a right one; it is a short element, with an asymmetrical expansion of the distal end. The medial portion is larger and expands more abruptly, almost at a right angle, whereas the lateral region expands in an obtuse angle. Specimen MPEF-PV 3148 is recognized as the proximal part of a coracoid, but it is otherwise uninformative.

Pelvic Girdle—An additional specimen, MPEF-PV 10901, includes an almost complete pelvic girdle prepared in dorsal view (Fig. 3B–C). All the bones are present, but the ilia are poorly preserved because the specimen was crushed during fossilization. In general aspect, the pelvic girdle is similar to specimen MPEF-PV 3135 described by Sterli and de la Fuente (2010). The pubis contacts the ischium posterolaterally, the ilium dorsally, and its counterpart in the midline. Anterolaterally, the pubis bears a lateral process that is half as long as the medial epipubic process. Anteromedially, the pubis shows a long, single ossified epipubic process as is developed by other basal Testudinata (i.e., *Pr. quenstedti*, *Pa. talampayensis*, *K. aprix*). The left ilium is a short bone (in comparison with the size of the ischium and pubis), and it seems to be slightly displaced from its natural position due to deformation. The right ilium, however, is better exposed in lateral view; it inclines posteriorly and expands distally to form an iliac blade. The ischium contacts the pubis anteriorly and seems to be in contact with the other ischium medially. The medial ischium-pubis contact precludes the midline merging of the well-developed thyroid fenestrae. Posterolaterally, the ischium develops a posterolateral, triangular process (= metischial process) that narrows distally. It is similar to the process recognized in *K. aprix*. Posteromedial to both ischia, a single, small element is also recognized. We interpret it as a remnant of a hypoischium. According to Gaffney (1990), the hypoischium is a bone that exhibits sexual dimorphism in *Pr. quenstedti*, being a single element in males and paired in females. The sutural contacts among both ischia and the hypoischium are clearly seen in this specimen (MPEF-PV 10901) and in MPEF-PV 10884. Only the right acetabulum is available for description, and it is roughly triangular in shape.

Forelimb—The humerus of specimen MPEF-PV 10884 is an almost complete right humerus, only missing the distal end (Figs. 2A–B, 3D–H). There are two other complete humeri preserved (MPEF-PV 1784 and 3149; Fig. 3I–L), two specimens where the proximal end is preserved (MPEF-PV 3151 and 3153), and another specimen where the distal portion is preserved (MPEF-PV 3150; Fig. 3M–Q). The humerus is a slender bone expanded at both ends (Fig. 3D–Q). It is more slender than in *Pr. quenstedti*, *Meiolania platyceps*, and *Gaffneylania auricularis*, but not as slender as in crown-group turtles. The proximal and distal ends are not in the same plane; there is a torsion between the two ends. The proximal end is expanded, the medial process being slightly bigger than the lateral process (Fig. 3D–L). The medial process is well developed, and is continuous with the nearly hemispherical head. In living turtles, the m. coracobrachialis magnus and subscapularis are attached to the medial process (Walker, 1973) and this is likely to be so in *Condorchelys* as well. Between the head and the lateral process, the shoulder is present. The lateral process is located below the medial process, and it has a ventral component. The m. supracoracoideus attaches to the lateral process (Walker,
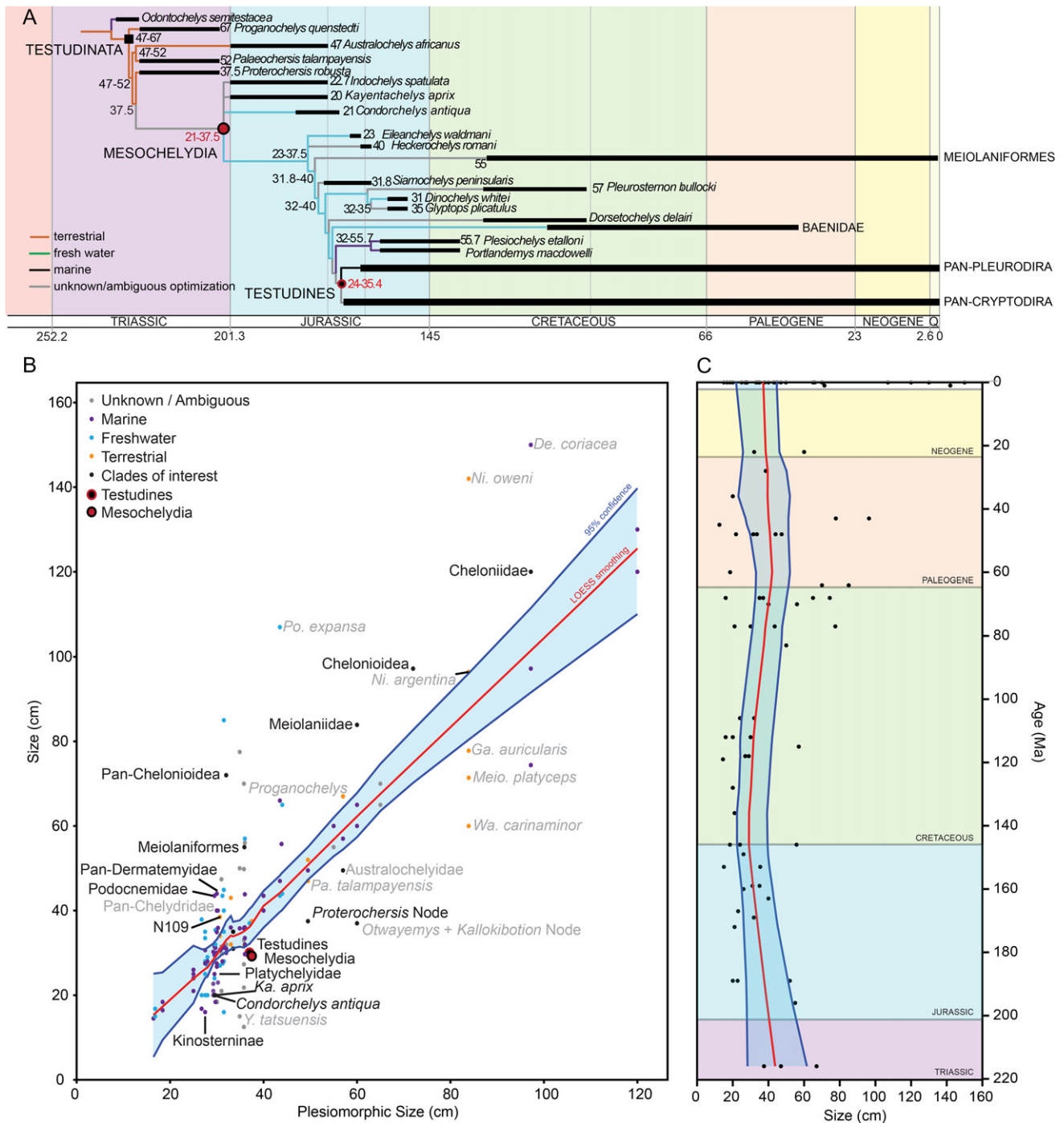
FIGURE 6. **A**, simplified strict consensus tree of the unconstrained analysis calibrated in time. The size and the habitat are optimized in the tree. **B**, graph showing the size (y) and plesiomorphic size (x) of taxa and nodes in centimeters. **C**, sizes of taxa and nodes (x) through time (y). Red line, LOESS regression analysis. Blue lines, 95% confidence interval of the regression analysis.

1973). Below the head and the shoulder, a slender deltopectoral crest is present. Laterally (anteriorly) to the deltopectoral crest, the m. deltoideus is attached (Walker, 1973), whereas medially (posteriorly) the m. latissimus dorsi and teres major are attached in a small concavity located below the head. In ventral view, the 'C'-shaped intertubercular fossa is present (Fig. 3F). The m. coracobrachialis brevis attaches to this fossa (Walker, 1973). Between the head and the medial process, there is a small concavity in the intertubercular fossa (Fig. 3F).

A similar concavity has been noticed in *Naomichelys speciosa* (Joyce et al., 2014); however, in this case, this depression (secondary intertubercular fossa) is located between the lateral process and the head. The shaft of the humerus is narrow (Fig. 3D–Q). Due to the compression suffered by the specimen, the sigmoidal curvature present in turtles is artifactually lost in this specimen. The m. triceps and brachialis inferior (Walter, 1973) attach to the dorsal and ventral surfaces of the shaft, respectively. In anterior view of the small part of the preserved distal

end, the groove leading to the ectepicondylar foramen is seen (Fig. 3J, N). The distal end of the humerus is better preserved in specimen MPEF-PV 3150 (Fig. 3M–Q). The distal end is expanded, but it is smaller than the expansion seen in the proximal end of the humerus of *C. antiqua* (MPEF-PV 3151, 3153, 10884). In dorsal view (Fig. 3I, J, L–N, P, Q), the distal end is formed by the entepicondyle and the ectepicondyle (posteriorly and anteriorly, respectively). The ectepicondyle is slightly larger than the entepicondyle, and it bears a groove that ends in the ectepicondylar foramen. Both condyles are separated by a median groove. In ventral view, the condyles for the articulation with the radius (capitullum) and the ulna (trochlea) are well differentiated (Fig. 3K, O). The trochlea (posterior) is slightly larger than the capitullum (anterior). Also in ventral view and above the double condyle, there is a concavity (maybe for muscle attachment).

Only the ?left radius is preserved in MPEF-PV 10884 (Fig. 2C, D), and it is consistent with the general morphology of radii among turtles. It is, however, an elongated bone, more slender than in *Pr. quenstedti*, *Pa. talamapayensis*, and *Naomichelys speciosa*. The radius has a round proximal end and an expanded distal end. The expansion of the distal end is twice the size of the proximal end, which articulated with the humerus and the ulna, whereas the distal did so with carpals and the ulna.

Hind Limb—Only the left femur is preserved in MPEF-PV 10884. It is seen in dorsal view (Fig. 2C–D), and resembles the femora of crown-group turtles. The femur is a slender and long bone, slightly longer than the humerus (4.8 and 4.3 cm, respectively). The proximal and distal ends are expanded. The femoral head is ovoid (1.6 times longer than wide), narrow, and proximodistally elongated. An elongated head of the femur is associated with aquatic habitats in turtles (Zug, 1971). In our specimen, only the trochanter minor is seen; it is well developed and connected with the head through a web of bone. The shaft is very slender (width of 0.4 cm in the narrower part), whereas the distal end bears two slightly differentiated condyles: the anterior for the tibia, the posterior for the fibula. The articulation of the tibia seems to be pointing slightly anteriorly, like in *Pr. quenstedti*. In dorsal view there is a medial depression between the condyles, likely a remnant of the intercondylar fossa (Gaffney, 1990).

Specimen MPEF-PV 3152 preserves only the proximal end of the right femur. The head and the trochanter minor are similar to specimen MPEF-PV 10884, but here the ventral surface can be observed showing shallow a depression that we regard as the intertrochanteric fossa, but it is possible that it is artifactual.

Only the left tibia is preserved in MPEF-PV 10884 and is seen in ventral view (Fig. 2C, D). It is a long element with both ends expanded. The proximal end is the most expanded, being twice as wide as the shaft. The distal end has a medial dome and a lateral flat surface interpreted as the articular surface for the astragalocalcaneum. The preservation of the specimen does not allow further description.

Only the left fibula is preserved in MPEF-PV 10884. It is seen only in ventral view (Fig. 2C, D). It is a long bone, relatively straight, with both ends expanded. A crest extending down the shaft and forming a distinct process is present. The distal end is the most expanded, and it is at least twice as wide as the shaft. The proximal end articulated with the femur and the distal end with the astragalocalcaneum.

Manus/Pes—A total of two metatarsals/metacarpals, two phalanges, and one ungual phalanx have been identified in specimen MPEF-PV 10884 (Fig. 2C, D). Unfortunately, due to the preservation of this specimen, we cannot associate any of them as belonging to the anterior or posterior autopodium.

There are two elements that can be recognized as metatarsals/metacarpals. One of them is a short, rectangular element showing an expanded end. Unfortunately, the other end is broken. The other metatarsal/metacarpal is a more slender element, and only the distal part is seen; no further details are available

Two short phalanges are preserved in specimen MPEF-PV10884 (Fig. 2C, D). These phalanges are preserved in dorsal view, and both have a long, ventral process at the proximal end of the phalanx that forms the ventral part of the articulation with the metatarsal/metacarpal. Only one ungual phalanx is recognized in this specimen. It is preserved in ventral view. It is a robust element, claw-like, not flattened. Due to the size, this ungual phalanx could belong to the second to forth digit from the manus or pes.

Caudal Region—Only one small chevron is preserved in specimen MPEF-PV 10884 (Fig. 2C, D). It has the typical 'V'-shaped outline. Due to the size of the chevron, we suggest that it corresponds to the anterior part of the tail. This is a viable match for the caudal vertebrae assigned to *Condorchelys antiqua* showing an articular surface for chevron bones (Sterli and de la Fuente, 2010).

A caudal vertebra is also recognized in specimens MPEF-PV 3149 (Fig. 3I–L) and 3158 (Fig. 4). The former could correspond to an anterior vertebra (because of the size and well-developed transverse process), whereas MPEF-PV 3158 could correspond to a more posterior vertebra (smaller in size). The caudal vertebrae are slightly amphicoelous or platycoelous. The centrum is longer than high. Its anterior articulating surface is circular in shape, being as high as wide. The transverse process is located in the middle of the centrum. In ventral view, the posterior part of the centrum shows the articular surfaces for the chevron. The neural arch is short, bearing well-developed postzygapophyses.

RESULTS OF PHYLOGENETIC ANALYSES

We performed several phylogenetic analyses in order to explore the phylogenetic relationships of turtles and, particularly, of *C. antiqua*. Our phylogenetic analyses followed different approaches to explore the effect of different methodologies and assumptions of the tree topology; we carried out three major analyses: (1) unconstrained morphological data alone using maximum parsimony; (2) constrained morphological data alone sing maximum parsimony; this analysis was in turn performed in two ways, using constrains derived from Guillon et al. (2012) and using constraints derived from Crawford et al. (2015); and finally (3) morphological and molecular total-evidence analysis using model-based Bayesian methods.

Maximum Parsimony Analyses

Morphology-Only, Unconstrained Analysis—Four thousand eight hundred most parsimonious trees of 895 steps were found (Supplementary Material 8). The consistency index (CI) and retention index (RI) are 0.345 and 0.772, respectively. A strict consensus was calculated, and it is shown in Supplementary Material 3. A summary of the main clades is shown in Figure 6A. The general topology of the consensus tree is similar to that of previously published ones (e.g., Sterli et al., 2015b), where crown clade Testudines is recovered monophyletic, with its two main crown clades (Cryptodira and Pleurodira) also monophyletic. Several taxa are located along the stem of Testudines, such as the Triassic turtles *Pr. quenstedti* and *Pa. talampayensis*, the Jurassic *K. aprix* and *H. romani*, and the clade Meiolaniformes, among others. *Condorchelys antiqua* is

recovered as a stem of Testudines in a polytomy together with *K. aprix* and *I. spatulata*, (Mesochelydia, clade 106; see node numbers in strict consensus tree shown in Supplementary Material 3). This polytomy is caused by the alternate positions of *K. aprix* and *C. antiqua* in the trees. The iterPCR analysis (Supplementary Material 3) suggests that the scoring of two characters (characters Pterygoid I and Plastron B) support alternate positions of these taxa in the trees. Potentially, the scoring of certain unknown characters in these two taxa and in *I. spatulata* will help to resolve their position (see Supplementary Material 3). This clade of basal turtles, including *C. antiqua*, is supported by two synapomorphies common to all trees (Supplementary Material 3) and with Bremer support of 2. These synapomorphies are the absence of supramarginal scales (character Supramarginal A) and the absence of anterior plastral tuberosities (character Extragular C). In some trees, this clade is also supported by other characters such as the presence of musk ducts (character Musk duct A), ligamentous connection between the plastron and the carapace (character Plastron A), and triradiate pectoral girdle (character Pectoral girdle A). See Supplementary Material 3 for the common synapomorphies for each clade.

The strict consensus has been calibrated using the information of the fossil record (Supplementary Material 3). The calibrated tree shows that Testudinata would have been originated 231 Mya (Carnian, Late Triassic), whereas Mesochelydia (clade 106) would have been originated 204 Mya (Rhaetian, Late Triassic). The calibration also shows that the Middle Jurassic is an important time for the evolution of turtles because the dates of origin of Testudines (171 Mya), Pan-Cryptodira (170 Mya; Bajocian), Cryptodira (167 Mya; Bathonian), and Pan-Pleurodira (165 Mya; Callovian) have been calculated to occur during that time. Among the main, more inclusive clades, only Pleurodira was estimated to originate in the Early Cretaceous (130 Mya; Hauterivian). For information on other nodes, see Supplementary Material 3.

Constrained Analysis Following Guillon et al. (2012)—Ten thousand trees (maximum number of trees allowed) of 918 steps were found using the molecular constraints of Guillon et al. (2012; Supplementary Material 9). These trees are 23 steps longer than the most parsimonious trees found in the unconstrained search. A strict consensus is provided in Supplementary Material 3. The general topology is similar to the unconstrained consensus tree, with the exception, of course, of the extant taxa and their closest extinct relatives.

The strict consensus of this analysis was also calibrated using the information of the fossil record (Supplementary Material 3). The results are very similar to those found in the unconstrained search. For instance, the dates of origin of Testudinata, Mesochelydia (clade 106), Pan-Pleurodira, and Pleurodira are the same in the unconstrained and in the constrained analysis (231, 204, 165, and 130 Mya, respectively). Small differences in results (between 2 and 3 Ma) exist in the calculation of the dates of origin of Testudines, Pan-Cryptodira, and Cryptodira, being 169, 168, and 164 Mya in the unconstrained analysis, all of them corresponding to the Middle Jurassic. For information on other nodes, see Supplementary Material 3.

Constrained Analysis Following Crawford et al. (2015)—Ten thousand trees (maximum number of trees allowed) of 924 steps were found using the molecular constraints of Crawford et al. (2015; Supplementary Material 10). These trees are 29 steps longer than the most parsimonious trees found in the unconstraint search. A strict consensus is provided in Supplementary Material 3. The general topology is similar to the unconstrained consensus tree, with the exception, of course, of the extant taxa and their closest extinct relatives.

The calibration of the strict consensus produced the same dates for the nodes of interest as the constrained analysis based on Guillon et al. (2012) topology. For information on other nodes, see Supplementary Material 3.

Bayesian Analysis

The results of this analysis are the most dissimilar of all. Testudinata, Testudines, Pan-Pleurodira, and Pan-Cryptodira are monophyletic as in the previous analyses (note that crown Pleurodira and Cryptodira were constrained) (Supplementary Materials 3 and 6). The tree presented is the maximum clade credibility (MCC), and the Harmonic mean of the likelihood is −27688.59. However, the stem of Testudines is much more populated than in the previous analyses because taxa usually considered pan-cryptodirans (e.g., xinjiangchelyids, sinemydids) are located in the stem of Testudines, as well as baenids, plesiochelyids, and meiolaniforms (Supplementary Material 3). On the other hand, the base of the turtle tree is similar to previous analyses, but the interrelationships inside some clades (e.g., Mesochelydia, clade 107) are resolved (Supplementary Material 3). There are other differences in the interrelationships of other clades (e.g., Platychelyidae, Durocryptodira), but the discussion of those differences is beyond the scope of this paper. For further information, see Supplementary Material 3.

Although there are evident differences between the Bayesian and cladistic analyses, the divergence times of Mesochelydia, Testudines, and Pan-Pleurodira are quite similar (Table 1). The origin of Mesochelydia is dated to the Late Triassic as in the cladistic analyses. Furthermore, the origin of Testudines and Pan-Pleurodira is dated to the Middle Jurassic as in the cladistic analyses. Note that because clades Pleurodira and Cryptodira were constrained for the node-dating Bayesian analysis, we do not discuss the ages of these clades, because it would be redundant.

Size Evolution

We mapped carapace length in the three cladistic analyses and in the tip-dating analysis in order to see the evolution of size depending on the phylogenetic context. For the sake of clarity, we are going to discuss the optimization of size in the seven nodes examined: Testudinata, Mesochelydia (node 106 of the unconstrained cladistic analysis), Testudines, Pan-Pleurodira, Pleurodira, Pan-Cryptodira, and Cryptodira. In Table 2, the optimization for each of the mentioned nodes in the four analyses is shown. The optimization of size in the remaining nodes can be found in Supplementary Material 3. As can be seen in Table 2, the optimization of size in the most basal node (Testudinata) we is interested in is the same for all the analyses (see also Supplementary Material 3). The optimization for Mesochelydia (node 106) is the same for the three cladistic analyses (21–37.5 cm), whereas it differs slightly from the optimization based on the topology found under Bayesian inference (31–37.5 cm). The minimum size for all the following clades and for all the analyses has been estimated to be 24 cm; however, some differences arise when maximum sizes are compared. Those differences are even bigger when the maximum sizes based on the unconstrained, parsimony analysis and on the Bayesian inference are compared. In Testudines, the maximum size was calculated to be 35.4 cm in the unconstrained phylogeny, whereas it was 32 cm in the Bayesian inference (Table 2). A similar situation was found in the optimization of pan-pleurodiran and pleurodiran nodes. The maximum size was calculated to be 35 cm in the unconstrained, parsimony analysis, whereas it was 26 cm for the Bayesian topology. Differences also exist in the optimization of maximum size in

TABLE 1. Calibration of selected clades in the different phylogenetic analyses performed in this study.

	Parsimony analysis			Tip-dating analysis
	Unconstrained	Constrained		
Node		Guillon et al. (2012)	Crawford et al. (2015)	
Testudinata	231	231	231	247
Mesochelydia	204	204	204	208
Testudines	171	169	169	171
Pan-Pleurodira	165	165	165	167.6
Pleurodira	130	130	130	–
Pan-Cryptodira	170	168	168	–
Cryptodira	167	164	164	–

TABLE 2. Optimization of size in selected clades in the different phylogenetic analyses performed in this study.

	Parsimony			Tip dating analysis
	Unconstrained	Constrained		
Node		Guillon et al. (2012)	Crawford et al. (2015)	
Testudinata	47–67	47–67	47–67	67
Mesochelydia	21–37.5	21–37.5	21–37.5	31–37.5
Testudines	24–35.4	24–33	24–33.5	24–32
Pan-Pleurodira	24–35	24–28	24–28	24–26
Pleurodira	24–35	24–28	24–28	24–26
Pan-Cryptodira	24–35.4	24–33	24–33.5	–
Cryptodira	24–40	24–33	24–33.5	24–32

the cryptodiran node. The maximum size calculated for this clade based on the unconstrained topology was 40 cm, whereas it was 32 in the Bayesian phylogeny.

Given that we are interested in discussing the evolution of size in the most basal nodes and the optimization in those nodes is congruent in the three analyses of MP, we are going to present our results based on Supplementary Material 3 (unconstrained analysis) and Figure 6B. The optimization of the node Testudinata gives a size range of 47–67 cm in the four analyses. In the next node (Australochelyidae node), there is a decrease in the maximum size to 52 cm. The size continues decreasing in the next node (*Proterochersis* node) to 37.5 cm. A significant drop in size occurs in the next node (Mesochelydia), with a size range of 21–37.5 cm. The *Proterochersis* and *Condorchelys* nodes fall outside the 95% confidence interval of the LOESS regression analysis shown in Figure 6B. In the next node (*Heckerochelys* node), there is a small increase in the minimum size to 23 cm. An increase in the size from 31.8 to 40 cm occurs in the next node (node 109). The estimated size range remains the same in the nodes located in the main axis and changes in the node Testudines where the size range is between 24 and 35.4 cm. Considerable increases in size in particular clades are observed in this analysis, such as in Meiolaniformes and crown Chelonioidea (this node falls outside the 95% confidence interval of the LOESS regression analysis shown in Fig. 6B). Furthermore, there are many examples of large-sized turtles documented in species not included in this cladistic analysis (e.g., several extant and extinct species of testudinids, some extinct chelids and podocnemidids such as *Stupendemys geographica*; Wood, 1976; Lapparent de Broin et al., 1993; Gaffney et al., 1998; Sánchez-Villagra and Scheyer, 2010).

The second analysis presented here was performed to test whether the differences between the final (N = 161, minimum size = 12.5 cm, maximum size = 150 cm, mean = 41.03 cm) and ancestral (N = 161, minimum size = 16.45 cm, maximum size = 120 cm, mean = 38.56 cm) sizes are significant. The results of the statistical analyses suggest that the sample does not have a normal distribution (final size: Shapiro-Wilk W = 0.7733, P = 1.66E-14; ancestral size: Shapiro-Wilk W = 0.6755, P = 2.22E-17) and that the two variables (final and ancestral sizes) are correlated (Spearman's r values = 5.74E-33). The LOESS smoothing 0.5 regression analysis is shown in Figure 6B. The node numbers can be found in Supplementary Material 3. The ancestral size for Testudinata (node 102) was estimated to be 57 cm. The following nodes (104, 103, 106) were recovered as significantly smaller than their respective ancestral nodes (Fig. 6B). Node 104 is significantly smaller (estimated carapace length [CL] = 49.5 cm) than its ancestral size (node 102). Node 103 is also significantly smaller (estimated CL = 37.5 cm) than its ancestral size (node 104). Furthermore, Mesochelydia (node 106) is also significantly smaller (estimated CL = 29.25 cm) than its ancestral size (node 103). In particular, *Condorchelys antiqua* (CL = 21 cm) is significantly smaller than the ancestral size for the clade. The same occurs with other members of that clade, such as *K. aprix* (CL = 20 cm) and *I. spatulata* (CL = 22.7 cm). *Eileanchelys waldmani* (CL = 23 cm) is also significantly smaller than its ancestral size (CL = 30.25 cm). On the other hand, *Heckerochelys romani* is significantly larger (CL = 40 cm) than its ancestral size. In node 109, there is an increase in the size (CL = 35.9 cm) compared with the ancestral size of node 107 (CL = 30.25 cm). The following nodes leading to Testudines maintain a similar size (CL = 35.9 cm), except in node 118 (Testudines) where again, a significant reduction in size occurs (CL = 29.7 cm). Inside Testudines, the average size remains more or less constant, with significant increases in size in some clades (e.g., Pan-Chelonioidea, Pan-Dermatemydidae, Podocnemididae) and significant decreases in size in other clades (e.g., Kinosterninae, Platychelyidae).

We plotted size through time (Fig. 6C). There is a general decrease in size during the Jurassic, and during the Cretaceous there is an increase that is maintained during the Paleogene. During the Neogene, size seem to remain the same or to diminish to a small extent.

From Land to Water, and Then to Land Again

We also mapped the 'habitat' of the turtles in the four analyses. Because the results are similar in the three analyses based on parsimony (Supplementary Material 3), we are going to base our discussion in the unconstrained-morphology-only analysis. 'Habitat' optimizes in Testudinata as terrestrial because the most basal members of the clade (e.g., *Pr. quenstedti*, *Pa. talampayensis*) and the outgroups (e.g., *Sphenodon punctatus*, *Anthodon serrarius*) are inferred to be terrestrial mainly based on anatomical features (e.g., relationship of the auto-, stylo-, and zeugopodia, paleohistology of dermal plates) (e.g., Rougier et al., 1995; Joyce and Gauthier, 2004; Scheyer, 2007). The optimization in Mesochelydia (node 106) is ambiguous because the habitat is not known for *I. spatulata* and is dubious for *K. aprix* (see Weldon and Gaffney, 1998; Scheyer, 2007). At the next node, this character optimizes as aquatic (from fresh water environments). The majority of the following nodes optimize as aquatic, with the exception of the clades Meiolaniidae and Testudinidae. There are other clades supposed to be terrestrial as well, but they were not included in this analysis (e.g., Solemydidae, Nanhsiungchelyidae). Ambiguity also exists near the node Testudines. This ambiguity is between freshwater and marine mainly; consequently, we can assume that the optimization is unambiguous regarding whether these turtles were aquatic. The ambiguity is due to the phylogenetic position of some turtles adapted to marine environments (e.g., *Notoemys*, plesiochelyids) and some others adapted to fresh water (e.g., pleurodires, 'macrobaenids'). A better understanding of the phylogenetic position of plesiochelyids, *Santanachelys gaffneyi*, and *Solnhofia parsonsi* would help to clarify the habitat at the base of Testudines.

Most of the ambiguity presented in the optimization of habitat in the parsimony analyses disappears in the Bayesian analysis (Supplementary Material 3). As in parsimony, the habitat at the base of the turtle tree optimizes as terrestrial and changes to aquatic (fresh water) in Mesochelydia (node 106). Then the main nodes optimize as aquatic, with the exception of several marine (e.g., Platychelyidae, Pan-Chelonioidea, plesiochelyids-eurysternids) and terrestrial (e.g., Meiolaniidae, Testudinidae) clades.

DISCUSSION

Calibration

Sterli et al. (2013) extensively discussed the different results for the calibration of Testudines, Pleurodira, and Cryptodira. In their study, the origin of Testudines and of Cryptodira was calculated to be in the Middle–Late Jurassic, whereas for Pleurodira it was in the Early Cretaceous. In a later paper, Joyce et al. (2013) used molecular clocks and obtained much older ages for those nodes. They estimated the origin of Testudines to be in the Late Triassic, the origin of Cryptodira in the Early Jurassic, and the origin of Pleurodira in the Middle Jurassic. Rodrigues and Diniz-Filho (2016), also using molecular clocks, found the origin of Testudines in the Late Jurassic and the origin of both Pleurodira and Cryptodira in the Early Cretaceous. On the other hand, the calibration of the composite phylogenetic tree based on morphology of Joyce et al. (2016) suggests that the origin of Testudines would have been in the Middle Jurassic, the origin of Cryptodira at the boundary between the Middle and Late Jurassic, and the origin of Pleurodira in the Early Cretaceous. Furthermore, recently, Pereira et al. (2017) published the largest, calibrated molecular phylogeny of turtles, suggesting that the origin of Testudines occurred in the Early Jurassic, the origin of Cryptodira

occurred in the Middle Jurassic, and the origin of Pleurodira occurred in the Late Jurassic.

Our cladistic analyses give more or less consistent results for all the main nodes discussed above. The origin of Testudines, Pan-Pleurodira, Pan-Cryptodira, and Cryptodira was calculated to be in the Middle Jurassic, whereas for Pleurodira it is calculated to be in the Early Cretaceous. As is common for molecular clock estimates, the dates calculated in our total-evidence Bayesian analysis are slightly older than those obtained from the morphological trees calibrated with the fossil record without the use of model approaches for dating nodes. All in all, although there are differences between all different analyses, the majority highlight the Jurassic as the key time for the origin and early diversification of crown-group turtles. The convergence in the dates obtained from parsimony and Bayesian methods is encouraging, underlining a rising consensus regarding the origin of these major taxa.

Heterochrony at the Base of the Turtle Tree

Because we are mainly interested in the node that contains *Condorchelys antiqua* (Mesochelydia; node 106), we are going to focus the discussion on that node. Above, we advanced the idea that turtles in node Mesochelydia show a significant reduction in size, a reduction that started at node 104. Some of the features present in the adult specimens of *C. antiqua*, *K. aprix*, and other more derived turtles are features present in juvenile specimens of extant turtles (e.g., small size, fontanelles in the shell). Because small size and miniaturization have been correlated with heterochronic changes (Angielczyk and Feldman, 2013), it is therefore possible that the early evolution of turtles (around node 106) could have been driven by heterochronic changes.

The modern definition of heterochrony, or specifically growth heterochrony (Smith, 2001:171), is related to changes in the timing of development. Alberch et al. (1979:306) defined that heterochronic changes "can be classified according to the nature of perturbations in growth parameters." Retarded processes (paedomorphosis) produce descendants with morphologies that resemble the juvenile stages of the ancestor (Alberch et al., 1979). In contrast, accelerated processes (peramorphosis) produce descendants with morphologies that transcend that of the ancestor (Alberch et al., 1979). In general, small-sized taxa are often paedomorphic, resulting in ontogenetic changes such as neoteny (e.g., growth rate slower than in the ancestor) and progenesis (e.g., shortening in the period of growth relative to the ancestor) (Alberch et al., 1979). In turtles, Kordikova (2000, 2002) was among the first researchers to highlight the role of heterochronic changes, and particularly paedomorphic reorganization, in the evolution of Testudinata. This author provides evidence from the ontogeny of the shell in extinct and extant turtles. Later, Angielczyk and Feldman (2013) explored the reduction of size in emydine turtles as a consequence of miniaturization caused by heterochronic changes during ontogeny.

Reduction in size also affects the morphology of an organism, producing three main modifications (Hanken and Wake, 1993): reduction and structural simplification, morphological novelty, and increase in morphological variability. In the following paragraphs, we present some evidence for each of these main modifications that occurred in Mesochelydia (node 106) and that could be correlated with the reduction in size in this part of the turtle tree.

Reduction and Structural Modification—Hanken and Wake (1993) attributed underdevelopment to loss of organs or organ systems, including the loss of bones and simplified and reduced morphology in adults. All turtles except the large forms from

the Late Triassic lose supratemporals (character 30), lose lacrimals (character 8), have an unpaired vomer (character 41), have a reduced processus interfenestralis of the opisthotic (character 81), have lost the palatal teeth or they are reduced (character 43), have a simplified pectoral girdle (triradiate) (character 216), lose the dorsal process of the epiplastra (character 218), lose the hypoischium or it is reduced (character 235), have a reduced number of peripherals and marginals (character 131), lose supramarginals (character 139), have a reduced number of inframarginals (character 180 and 181), among others. Some of these characters optimize ambiguously in Mesochelydia (node 106) (e.g., characters 8, 30, 41, 81, 131) because they are unknown for some of the taxa involved in this polytomy (Supplementary Material 3).

Morphological Novelty—Hanken and Wake (1993) found a consistent association between significant phylogenetic body size decrease and morphological novelty in several taxa. Among morphological novelties, they cite negative allometry between a structure and size. The presence of a well-developed cavum tympani and its subsequent reorganization of the otic capsule (later followed by the development of the trochlear system) is characteristic of turtles included in Mesochelydia (node 106). An incipient development of the cavum tympani is present in *Pa. talampayensis* and *Australochelys africanus* but absent in *Pr. quenstedti*. In crown turtles, the otic capsule is reorganized and the adductor muscle is deviated from its course through the trochlear system located in the otic capsule in pan-cryptodirans and some stem turtles (e.g., meiolaniforms) and on the pterygoid in pan-pleurodiran turtles.

Increase in Morphological Variability—Evolutionary novelty produces a subsequent diversification that allows, in turn, the occupation of new ecological niches, for example, aquatic niches. If we map the habitat of extant and extinct turtles on a phylogeny (Supplementary Material 3), it is evident that the majority of the species of the clade are aquatic (fresh water) and few clades are terrestrial (e.g., meiolaniids, testudinids) or marine (e.g., chelonioids, platychelyids). It is noteworthy that the most basal turtles (*Pr. quenstedti*, *Proterochersis robusta*, *Pa. talampayensis*) would have been terrestrial (Rougier et al., 1995; Joyce and Gauthier, 2004; Scheyer and Sander, 2007) and then (certain for node 107, ambiguous for node 106) they would have made an incursion into the aquatic niche (see Supplementary Material 3; Anquetin, 2011) where they diversified greatly.

CONCLUSIONS

Condorchelys antiqua from Patagonia is currently the best-known Early–Middle Jurassic turtle from Gondwana. The new specimens not only corroborate the anatomy previously described for the species (e.g., anatomy of the basicranium) but also provide new information about poorly known or unknown parts of the skeleton (e.g., anatomy of the maxilla, anterior carapace, plastron, limb bones).

In agreement to previous studies, *C. antiqua* clusters with *K. aprix* and *I. spatulata* near the base of the turtle tree in a more derived position than the Triassic–Early Jurassic large terrestrial turtles. The calibration of the various phylogenetic analyses presented here suggests that the Jurassic is an important period for the origin and evolution of the main clades of turtles: Testudines, Pan-Pleurodira, Pan-Cryptodira and Cryptodira in particular. The available evidence suggests that the origin of crown Pleurodira would have occurred in the Early Cretaceous.

Summarizing, we suggest that heterochronic changes (paedomorphosis) might have governed the early evolution of turtles (clade Mesochelydia), resulting in turtles of smaller size, retaining features present in juveniles (e.g., presence of fontanelles), reducing or losing structures (e.g., loss of bones, loss of scutes), producing morphological novelties (e.g., development of the cavum tympani and concomitant muscular rearrangement), and increasing morphological variability, allowing the occupation of new ecological niches (e.g., aquatic niche). The calibrated trees show that this node would have appeared between 224.7 and 204 Mya (Norian–Rhaetian). More studies and better materials, particular of groups belonging to the stem, are necessary to further explore and test the role of heterochronic, paedomorphic in particular, features during the early evolution of turtles.

LITERATURE CITED

Alberch, P., S. J. Gould, G. F. Oster, and D. B. Wake. 1979. Size and shape in ontogeny and phylogeny. Paleobiology 5:296–317.

Angielczyk, K. D., and C. Feldman. 2013. Are diminutive turtles miniaturized? The ontogeny of plastron shape in emydine turtles. Biological Journal of the Linnean Society 108:727–755.

Anquetin, J. 2010. The anatomy of the basal turtle *Eileanchelys waldmani* from the Middle Jurassic of the Isle of Skye, Scotland. Earth and Environmental Science Transactions of the Royal Society of Edinburgh 101:67–96.

Anquetin, J. 2011. Evolution and palaeoecology of early turtles: a review based on recent discoveries in the Middle Jurassic. Bulletin de la Société géologique de France 182:235–244.

Anquetin, J., P. M. Barrett, M. E. H. Jones, S. Moore-Fay, and S. E. Evans. 2009. A new stem turtle from the Middle Jurassic of Scotland: new insights into the evolution and palaeoecology of basal turtles. Proceedings of the Royal Society B: Biological Sciences 276:879–886.

Beck, R. M. D., and M. S. Lee. 2014. Ancient dates or accelerated rates? Morphological clocks and the antiquity of placental mammals. Proceedings of the Royal Society of London B: Biological Sciences 281:20141278. doi: 10.1098/rspb.2014.1278.

Beck, R. M. D., N. M. Warburton, M. Archer, S. J. Hand, and K. P. Aplin. 2016. Going underground: postcranial morphology of the early Miocene marsupial mole *Naraboryctes philcreaseri* and the evolution of fossoriality in notoryctemorphians. Memoirs of Museum Victoria 74:151–171.

Cerda, I. A., J. Sterli and T. M. Scheyer. 2016. Bone shell microstructure of *Condorchelys antiqua* Sterli, 2008, a stem turtle from the Jurassic of Patagonia. Comptes Rendus Palevol 15:128–141.

Crawford, N. G., J. F. Parham, A. B. Sellas, B. C. Faircloth, T. C. Glenn, T. J. Papenfuss, J. B. Henderson, M. H. Hansen, and H. B. Simison. 2015. A phylogenomic analysis of turtles. Molecular Phylogenetic and Evolution 83:250–257.

Cúneo, R., J. R. Ramezani, R. Scasso, D. Pol, I. Escapa, A. M. Zavattieri, and S. Bowring. 2013. High-precision U-Pb geochronology and a new chronostratigraphy for the Cañadón Asfalto Basin, Chubut, central Patagonia: implications for terrestrial

faunal and floral evolution in Jurassic. Gondwana Research 24:1267–1275.

Datta, P. M., P. Manna, S. C. Ghosh, and D. P. Das. 2000. The first Jurassic turtle from India. Palaeontology 43:99–109.

Dos Reis, M. 2016. Notes on the birth–death prior with fossil calibrations for Bayesian estimation of species divergence times. Philosophical Transactions of the Royal Society of London B: Biological Sciences 371:20150128. doi: 10.1098/rstb.2015.0128.

Gaffney, E. S. 1990. The comparative osteology of the Triassic turtle *Proganochelys*. Bulletin of the American Museum of Natural History 194:1–263.

Gaffney, E. S. 1996. The postcranial morphology of *Meiolania platyceps* and a review of the Meiolaniidae. Bulletin of the American Museum of Natural History 229:1–165.

Gaffney, E. G., and F. A. Jenkins. 2010. The cranial morphology of *Kayentachelys*, an Early Jurassic cryptodire, and the early history of turtles. Acta Zoologica 11:35–68.

Gaffney, E. S., K. E. Campbell, and R. C. Wood. 1998. Pelomedusoid side-necked turtles from Late Miocene Sediments in southwestern Amazonia. American Museum Novitates 3245:1–12.

Gaffney, E. S., J. H. Hutchison, F. A. Jenkins, and L. J. Meeker. 1987. Modern turtle origins: the oldest known cryptodire. Science 237:289–292

Gaffney, E. S., T. H. Rich, P. Vickers-Rich, A. Constantine, R. Vacca, and L. Kool 2007. *Chubutemys*, a new eucryptodiran turtle from the Early Cretaceous of Argentina, and the relationships of the Meiolaniidae. American Museum Novitates 3599:1–35.

Goloboff, P., J. Farris, and K. Nixon. 2008. A free program for phylogenetic analysis. Cladistics 24:774–786.

Guillon, J.-M., L. Guéry, V. Hulin, and M. Girondot. 2012. A large phylogeny of turtles (Testudines) using molecular data. Contributions to Zoology 81:147–158.

Hammer, O., D. A. T. Harper, and P. Ryan. 2001. PAST: paleontological statistics software package for education and data analysis. Palaeontolologia Electronica 4:1–9 https://palaeo-electronica. org/2001_1/past/issue1_01.htm.

Hanken, J., and D. B. Wake. 1993. Miniaturization of body size: organismal consequences and evolutionary significance. Annual Review of Ecology and Systematics 24:501–519.

Heath, T. A., J. P, Huelsenbeck, and T. Stadler. 2014. The fossilized birth–death process for coherent calibration of divergence-time estimates. Proceedings of the National Academy of Sciences of the United States of America 111:E2957–E2966.

Joyce, W. G. 2007. Phylogenetic relationships of Mesozoic turtles. Bulletin of the Peabody Museum of Natural History 48:3–102.

Joyce, W. G. 2017. A Review of the Fossil Record of Basal Mesozoic Turtles. Bulletin of the Peabody Museum of Natural History 58:65–113.

Joyce, W. G., and J. A. Gauthier. 2004. Palaeoecology of Triassic stem turtles sheds new light on turtle origins. Proceedings of the Royal Society of London B: Biological Sciences 271:1–5.

Joyce, W. G., J. F. Parham, and J. A. Gauthier. 2004. Developing a protocol for the conversion of rank-based taxon names to phylogenetically defined clade names, as exemplified by turtles. Journal of Paleontology 78:989–1013.

Joyce, W. G., J. Sterli, and S. Chapman. 2014. The skeletal morphology of the solemydid turtle *Naomichelys speciosa* from the Early Cretaceous of Texas. Journal of Paleontology 88:1257–1287.

Joyce, W. G., M. Rabi, J. Clark, and X. Xu. 2016. A toothed turtle from the Late Jurassic of China and the global biogeographic history of turtles. BMC Evolutionary Biology 16:236.

Joyce, W. G., J. F. Parham, T. R. Lyson, R. C. M. Warnock, and P. C. J. Donoghue. 2013. A divergence dating analysis of turtles using fossil calibrations: an example of best practices. Journal of Paleontology 87:612–634.

Klein, I. T. 1760. Classification und kurze Geschichte der vierfüszigen Thiere (translation by F. D. Behn). Jonas Schmidt, Lübeck.

Kordikova, E. G. 2000. Paedomorphosis in the shell of fossil and living turtles. Neues Jahrbuch für Geologie und Paläontologie, Abhandlungen 218:399–446.

Kordikova, E. G. 2002. Heterochrony in the evolution of the shell of Chelonia. Part 1: terminology, Cheloniidae, Dermochelyidae, Trionychidae, Cyclanorbidae and Carettochelyidae. Neues Jahrbuch für Geologie und Paläontologie, Abhandlungen 226:317–343.

Khosatzky, L. I. 1997. Big turtle of the Late Cretaceous of Mongolia. Russian Journal of Herpetology 4:148–154.

Lanfear, R., B. Calcott, S. Y. Ho, and S. Guindon. 2012. PartitionFinder: combined selection of partitioning schemes and substitution models for phylogenetic analyses. Molecular Biology and Evolution 29:1695–1701.

Lapparent de Broin, F., J. de Bocquentin, and F. R. Negri. 1993. Gigantic turtles (Pleurodira, Podocnemididae) from the Late Miocene–Early Pliocene of southwestern Amazon. Bulletin de l'Institut Francais des Études Andines 22:657–670.

Lewis, P. O. 2001. A likelihood approach to estimating phylogeny from discrete morphological character data. Systematic Biology 50:913–925.

López-Conde, O. A., J. Sterli, J. Alvarado-Ortega, and M. L. Chavarría-Arellano. 2017. A new platychelyid turtle (Pan-Pleurodira) from the late Jurassic (Kimmeridgian) of Oaxaca, Mexico. Papers in Palaeontology 3:161–174.

Miller, M. A., W. Pfeiffer, and T. Schwartz. 2010. Creating the CIPRES Science Gateway for inference of large phylogenetic trees. Gateway Computing Environments Workshop 2010:1–8.

Pereira, A. G., J. Sterli, F. R. Moreira, and C. G. Schrago. 2017. Multilocus phylogeny and statistical biogeography clarify the evolutionary history of major lineages of turtles. Molecular Phylogenetics and Evolution 113:59–66.

Pol, D., and I. Escapa. 2009. Unstable taxa in cladistic analysis: identification and the assessment of relevant characters. Cladistics 25:515–527.

Pol, D., and M. A. Norell. 2006. Uncertainty in the age of fossils and the stratigraphic fit to phylogenies. Systematic Biology 55:512–521.

Pyron, R. A. 2016. Novel approaches for phylogenetic inference from morphological data and total-evidence dating in squamate reptiles (lizards, snakes, and amphisbaenians). Systematic Biology 66:38–56. doi:https://doi.org/10.1093/sysbio/syw068

Rauhut, O. W. M., T. Martin, E. Ortiz-Jaureguizar, and P. Puerta. 2002. A Jurassic mammal from South America. Nature 416:165–168.

Rodrigues, J. F. M., and J. A. F. Diniz-Filho. 2016. Ecological opportunities, habitat, and past climatic fluctuations influenced the diversification of modern turtles. Molecular Phylogenetics and Evolution 101:352–358.

Ronquist, F., M. Teslenko, P. van der Mark, D. L. Ayres, A. Darling, S. Höhna, and J. P. Huelsenbeck. 2012. MrBayes 3.2: efficient Bayesian phylogenetic inference and model choice across a large model space. Systematic Biology 61:539–542.

Rougier, G. W., M. S. de la Fuente, and A. B. Arcucci. 1995. Late Triassic Turtles from South America. Science 268:855–858.

Rougier, G. W., A. Garrido, L. Gaetano, P. F. Puerta, C. Corbitt, and M. J. Novacek. 2007. First Jurassic triconodont from South America. American Museum Novitates 3580:1–17.

Sánchez-Villagra, M. R., and T. M. Scheyer. 2010. Fossil turtles from the northern neotropics: the Urumaco sequence fauna and finds from other localities in Venezuela and Colombia; pp. 173–191 in M. R. Sánchez-Villagra, O. A. Aguilera, and A. A. Carlini (eds.), Urumaco and Venezuelan Paleontology. Indiana University Press, Bloomington, Indiana.

Scheyer, T. M. 2007. Comparative bone histology of the turtle shell (carapace and plastron): implications for turtle systematics, functional morphology, and turtle origins. Doctoral dissertation, Mathematisch-Naturwissenschaftliche Fakultät, Universität Bonn, Bonn, Germany, 343 pp. http://hss.ulb.uni-bonn.de/2007/1229/1229.htm.

Scheyer, T. M., and P. M. Sander. 2007. Shell bone histology indicates terrestrial palaeoecology of basal turtles. Proceedings of the Royal Society B: Biological Sciences 274:1885–1893.

Smith, K. K. 2001. Heterochrony revisited: the evolution of developmental sequences. Biological Journal of the Linnean Society 73:169–186.

Sterli, J. 2008. A new, nearly complete stem turtle from the Jurassic of South America with implications for turtle evolution. Biology Letters 4:286–289.

Sterli, J. 2010. Phylogenetic relationships among extinct and extant turtles: the position of Pleurodira and the effects of the fossils on rooting crown-group turtles. Contributions to Zoology 79:93–106.

Sterli, J., and M. S. de la Fuente. 2010. Anatomy of *Condorchelys antiqua* Sterli 2008, and the origin of the modern jaw clousures mechanism in turtles. Journal of Vertebrate Paleontology 30:1–15.

Sterli, J., and W. G. Joyce. 2007. The cranial anatomy of the Early Jurassic turtle *Kayentachelys aprix*. Acta Palaeontologica Polonica 52:675–694.

Sterli, J., M. S. de la Fuente, and G. W. Rougier. 2015a. The "Rosetta Stone" for deciphering the anatomy of the stem turtle *Condorchelys antiqua* (Early-Middle Jurassic; Chubut, Argentina). PeerJ PrePrints 3:e884v1. doi: 10.7287/peerj.preprints.884v1.

Sterli, J., M. S. de la Fuente, and J. M. Krause. 2015b. A new turtle from the Palaeogene of Patagonia (Argentina) sheds new light on the diversity and evolution of the bizarre clade of horned turtles (Meiolaniidae, Testudinata). Zoological Journal of the Linnean Society 174:519–548.

Sterli, J., D. Pol, and M. Laurin. 2013. Incorporating phylogenetic uncertainty on phylogeny-based palaeontological dating and the timing of turtle diversification. Cladistics 29:233–246.

Stipanicic, P. N., F. Rodrigo, O. L. Baulies, and C. G. Martínez. 1968. Las formaciones presenonianas en el denominado Macizo Nordpatagónico y regiones adyacentes. Revista de la Asociación Geológica Argentina 23:67–98.

Sukhanov, V. B. 2006. An archaic turtle, *Heckerochelys romani* gen. et sp. nov., from the Middle Jurassic of Moscow region, Russia; pp. 104–111 in I. G. Danilov and J. F. Parham (eds.), Fossil Turtle Research. Russian Journal of Herpetology. volume 1, number 13(Suppl.).

Vlachos, E., and M. Rabi. 2017. Total evidence analysis and body size evolution of extant and extinct tortoises (Testudines: Cryptodira: Pan-Testudinidae). Cladistics. doi: 10.1111/cla.12227.

Volkheimer, W., M. E. Quattrocchio, N. G. Cabaleri, P. L. Narváez, U. Rosenfeld, L. Scafati, and D. L. Melendi. 2015. Environmental and climatic proxies for the Cañadón Asfalto and Neuquén basins (Patagonia, Argentina): review of Middle to Upper Jurassic continental and near coastal sequences. Revista Brasileira de Paleontologia 18:71–82.

Walker, W., Jr. 1973. The locomotor apparatus of Testudines; pp. 1–100 in C. Gans (ed.), Biology of the Reptilia 4. Academic Press, London and New York.

Weldon, P. J., and E. S. Gaffney. 1998. An ancient integumentary gland in turtles. Naturwissenschaften 85:556–557.

Wood, R. C. 1976. *Stupendemys geographicus*, the world's largest turtle. Breviora 436:1–31.

Zhang, C., T. Stadler, S. Klopfstein, T. A. Heath, and F. Ronquist. 2015. Total-evidence dating under the fossilized birth-death process. Systematic Biology 65:228–249. https://doi.org/10.1093/sysbio/syv080.

Zug, G. 1971. Buoyancy, locomotion, morphology of the pelvic girdle and hindlimb, and systematics of cryptodiran turtles. Miscellaneous Publications Museum of Zoology, University of Michigan 142:5–98.

APPENDIX 1. Measurements of *Condorchelys antiqua*.

MPEF-PV 10884	
Straight length of carapace	21 cm (estimated)
Width of carapace	16 cm (estimated)
Length of plastron	15 cm (estimated)
Length of femur	4.8 cm
Length of tibia	3.35 cm
Length of fibula	3.3 cm
Length of humerus	4.3 cm (estimated)
Length of radius	2.1 cm
Length of metatarsal/metacarpal	1 cm
Length of phalanges	0.7 cm
Length of ungual phalanx	0.9 cm
MPEF-PV 3132	
Preserved length of the carapace (measured in the midline)	15.2 cm
Estimated length of the carapace	21.2 cm
Estimated width of the carapace	16 cm
MPEF-PV 1784	
Length of humerus	4.1 cm
MPEF-PV 3149	
Length of humerus	4.6 cm